ABSTRACT

Title of Thesis: Performance measurement and scaling in small internal combustion engines.

Shyam Kumar Menon
Master of Science, 2006

Thesis Directed By: Assistant Professor Christopher P. Cadou
Department of Aerospace Engineering

Small hobby engines with masses less than 1 kg are attractive for use in low cost unmanned air vehicles (UAVs) because they are mass produced and inexpensive, however very little information about their performance is available in the scientific literature. This thesis describes the development of a dynamometer system suitable for measuring the power output and efficiency of these small engines and presents detailed performance measurements for a particular engine with a mass of 150 grams that could be suitable for powering a low-cost UAV. The performance of the engine was found to improve considerably by controlling the fuel-air mixture. The objective is to use the dynamometer system to collect data that provides insight into the processes/loss mechanisms governing small engine performance so that it may be improved and to develop scaling laws for the performance of engines in the 20 g to 1 kg range that may be used by designers of low-cost UAVs.

Performance Measurement and Scaling in Small Internal Combustion Engines.

By

Shyam Kumar Menon

Thesis submitted to the Faculty of the Graduate School of the
University of Maryland, College Park, in partial fulfillment
of the requirements for the degree of
[Master of Science]
[2006]

Advisory Committee:
Assistant Professor Christopher Cadou, Chair
Associate Professor Kenneth Yu
Associate Professor Gregory Jackson

© Copyright by
[Shyam Kumar Menon]
[2006]

Dedication

To my parents, my sister and

To my friends

Acknowledgements

There are a number of people who have been of help and inspiration to me in my graduate work and I would like to thank them for their assistance.

I would like to thank my advisor Dr.Christopher Cadou for his guidance and support. I would like to thank my labmates Kiran Dellimore, Timothy Leach and Anand Veeraragavan who have been great friends and supportive people in all my time here in grad school. I would like to thank Nathan Moulton who laid the foundations for this project and built the initial rig.

I would like to thank Minor Appleman and Vince Castelli of the Naval Surface Warfare Center Carderock Division (NSWCCD) for partially supporting this work. I would also like to thank the MAV MURI project (Grant No. ARMY-W911NF0410176) and Technical Monitor Dr. Gary Anderson for continued support of this research effort.

Table of Contents

List of Tables

List of Figures

Nomenclature

f_a , f_m	Atmospheric factor and engine factor
$\vec{F}$	Force
I	Moment of inertia
k_{lc}	Stiffness of the load cell
L/D	Lift/drag ratio of the vehicle
m	Mass of the additional weight added to the engine cradle
$\dot{m}$	Mass flow rate
MW	Molecular Weight
N_{nat}	Engine speed associated with the natural frequency of the cradle-load cell system
p, p_r	Test pressure and standard reference pressure
p_{sr} , p_s	Test saturated water vapor pressure and standard reference saturated water vapor pressure
P	Measured output power
P_r	Corrected power under standard reference conditions
q	Fuel mass per cycle per liter of air
q_c	Corrected specific fuel delivery
Q_r	Heating value
r	Distance between added mass and cradle axis of rotation
r_r	Boost pressure ratio
R	Length of the moment arm

T_r, T	Test ambient air temperature and standard reference ambient air temperature
Γ	Measured engine torque
ω	Engine speed
η	Efficiency
δ_{max}	Maximum deflection of the load cell
θ_e	Angle of cradle associated with steady state operation
ω_n	Natural frequency of the system
β	Overall damping coefficient for cradle bearings
ρ	Density of air, mixture, methanol, nitromethane and castor oil
χ	Volume fraction of methanol, nitromethane and castor oil in the fuel
α_c	Atmospheric correction factor
ϕ_r, ϕ	Test relative humidity and standard reference relative humidity
χ_f	Fuel mass fraction at takeoff

Subscripts

a	Air
c	Cradle
e	Engine
f	Fuel

lc	Load cell
o	Overall
p	Propulsive
th	Thermal
CH_3OH	Methanol
CH_3NO_2	Nitromethane
Oil	Castor oil

Chapter 1: Introduction

1.1 Unmanned Air Vehicles.

1.1.1 Uses, Applications and types.

Unmanned air vehicles represent a rapidly growing segment of the aerospace industry with myriad applications. These include high-altitude imagery, border patrol, maritime surveillance, environmental sensing, media reporting and law enforcement. As a result, these vehicles are set to become significant components of military, civil and even commercial aviation. A recent study has proposed a variety of changes for the National Airspace system to incorporate these new and emerging technologies[1].

These vehicles are often classified based on mission requirements[2]. Short range, low altitude, tactical UAV's operate at altitudes up to 10,000 ft with a range of about 500 km (4 hours). One example of a short range low altitude vehicle is a low-cost UAV called 'Silver Fox'[3] being manufactured for the US Navy by Advanced Ceramics Research Inc. Medium altitude long endurance UAV's operate at altitudes from 25,000 to 40,000 ft with a range of about 150-1500 km (5-25 hours). Examples include the MQ-5B Hunter developed by Northrop Grumman[4]. High altitude long endurance UAV's operate at altitudes above 40,000 ft with a range more than 2000 km (10 hours and more). Examples include the Global Hawk RQ-4A with a range of more than 20,000 km and a maximum endurance of about 35 hours[4].

Micro-Air Vehicles or (MAVs) are a smaller line of unmanned aircraft that weigh less than about 200 g. They are equipped with a variety of sensors but at present are only able to fly for about 30 minutes because of their limited ability to

carry energy on board the vehicle. These are intended to be man-portable and to serve a variety of military and civilian functions ranging from battlefield reconnaissance to environmental monitoring. They can be used singly or deployed in multiple-vehicle networked configurations[5]. Developmental programs for these vehicles have been the focus of several government sponsored research activities[6- 8] that aim to deliver the technology in a 3-5 year time-frame.

1.1.2 Development challenges for MAV's.

Development of Micro Air Vehicles faces several grand challenges. The first is miniaturization of the entire payload which would consist, typically, of a guidance and control system coupled to a GPS-based positioning system for autonomous operation, and a telemetry system to relay the desired data to personnel on the ground. This is in addition to the mission payload that includes sensors and cameras. The second challenge is to develop airframes and propulsion systems that are efficient at small scales. This is difficult because Reynolds numbers associated with micro-air vehicle flight are several orders of magnitude smaller than those associated with conventional flight. This in turn, lowers the aerodynamic efficiency of lift-generating systems for micro-air vehicles compared to their conventional-scale counterparts[9-10]. The third challenge is developing efficient miniaturized power and propulsion systems. These must be capable of storing and converting energy efficiently to provide mechanical and/or electrical power for the propulsion and payload systems.

1.2 Power/Propulsion Challenge.

The primary objective in developing power and propulsion systems for UAV's is to maximize either range or endurance. The Brequet range equation for a fixed-wing aircraft[11] shows that the critical aspects of the power system that govern the range and/or endurance are its overall thermal efficiency (η_{th}) and the energy per unit mass (or energy storage efficiency) of the fuel (Q_r):

$$R = \eta_p \eta_{th} \frac{Q_r}{g} \frac{L}{D} \ln(1+\chi) \tag{1}$$

The other terms in this expression describe aspects of the vehicle that are independent of the propulsion system. These include the efficiency of the propeller or other propulsive device (η_p), the acceleration of gravity (g), the airframe's lift-to-drag ratio (L/D), and the ratio of the fuel weight to the empty weight of the vehicle (χ).

Figure 1 shows contours of range as a function of energy density of the fuel (Q_r) and overall thermal efficiency (η_o) for a 'typical' small UAV patterned after the 'Low-cost Unmanned Air Vehicle' being developed by the US navy. The symbols on the figure correspond to various candidate power systems: batteries, direct methanol fuel cells, and methanol-fueled small internal combustion engines. The figure shows that the range target of 1500 miles (2414 km) can be achieved by switching from batteries to higher energy density liquid hydrocarbon fuels like JP10 that can store 50 times more energy than batteries. However, the figure also show that the energy density advantage of liquid hydrocarbon fuels over batteries can only be realized if

the conversion device(i.e the engine) is capable of converting the stored energy with 'reasonable' efficiency- in this case 25%.

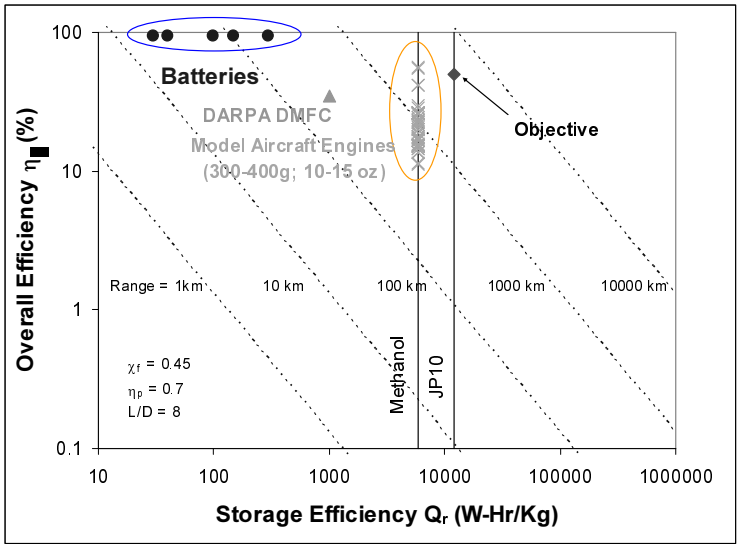

Figure 1 Range of a low-cost UAV as a function of the energy density of its fuel Q_r (storage efficiency) and the overall efficiency of the power plant. The calculation is based on the Brequet range equation assuming a takeoff fuel mass fraction χ_f=0.45, a propulsive efficiency of η_p=0.7 and L/D=8.

While the data points in figure 1, corresponding to small model aircraft engines (crosses, computed from manufacturer's reported performance) indicate that the target efficiency may be obtainable, the Navy faces several challenges. First, the large scatter in performance reported by manufacturer raises questions about its reliability. Second, model aircraft engines do not operate on the right fuel (a fuel already present in the logistic chain). Because it is difficult to mix fuel and air efficiently at small scales, model aircraft engines consume special oxygenated fuels that are mixtures of methanol, nitro-methane and castor oil. These engines would need to be converted to operate on higher energy density tactical fuels like JP10 to meet the range requirement and to ensure compatibility with ship-board operations. Third, there is some evidence to suggest that engine efficiency does not scale

favorably with size. Figure 2 shows estimates of small engine efficiency made from manufacturer's reported power output as a function of the size (mass) of the engine. It shows that efficiency decreases as the size of the engine is reduced. This makes some qualitative sense as one would expect the relative importance of thermal and frictional losses in engines to scale with the engine's surface-to-volume ratio which increases as the size of the engine is reduced.

However, the log-linear scaling of efficiency with engine size breaks down for smaller engines with masses less than 1 kg (35 oz). This could be a consequence of the fundamental physical limitations of the internal combustion engine[12-13].

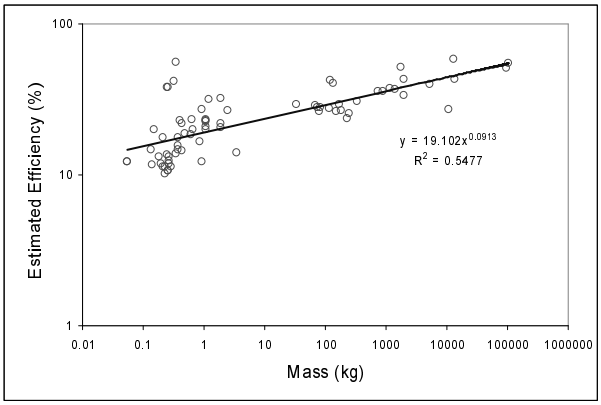

Figure 2 Efficiency vs. engine size for a range of piston IC engines[14].

1.3 Motivation and objectives of thesis.

1.3.1 Motivation.

Figure 1 shows that liquid hydrocarbon-fueled engines could enable large improvements in range and/or endurance over present battery-based technologies provided that they can achieve 'reasonable' operating efficiencies. Unfortunately, reliable performance data is not available from manufacturers so the efficiency of these engines is largely unknown. Acquiring reliable performance data for a range of

small engines would be useful for several reasons. First, it would define the current 'state of the art' thereby enabling us to understand exactly what we can and cannot do today with today's technology. Second, it would provide the data necessary for producing optimized UAV platforms so that we can take maximum advantage of the technology available today. Third, it would enable us to understand how to improve the current technology by identifying the factors that limit performance and by providing an overall understanding of how engine performance scales with size so that we do not try to construct power systems that are the wrong size for the application.

1.3.2 Overall objectives of Thesis.

The principal objective of this thesis is to develop a system that is capable of measuring the performance (ie. power output and fuel efficiency) of a wide range of model aircraft engines. The secondary objective is to use this system to understand the factors that limit the performance of particular engines and, by measuring the performance of several engines, obtain an understanding of how one should expect small engine performance to scale with engine size. Given the challenges associated with measuring performance of small engines, our objective is to determine power output and efficiency to within 5% of their nominal values. This level of accuracy is adequate for guiding engine selection for low-cost UAV's. It should also provide adequate discrimination between engines of different sizes so that scaling laws can be identified.

1.4 Approach.

The approach that we will take here is to develop a dynamometer that is capable of making reliable measurements of torque, engine speed, and fuel consumption. These are the critical measurements for determining an engine's power output and fuel efficiency. However, to understand the operation of the engine and to help explain the power and efficiency data, measurements of other engine operating parameters like fuel/air ratio, engine operating temperature, throttle position and mixture setting are also important. Care will be taken to establish the reliability of the measurements through an uncertainty analysis and multiple experiments by which to establish the instrument's repeatability. This will be accomplished by operating the dynamometer with a single engine. Once the reliability of the instrument has been established, it will be used to acquire preliminary performance data for two other engines each of a different size. These measurements will enable some preliminary conclusions to be drawn about the factors that limit engine performance and how engine performance scales with engine size. Finally, recommendations for how the measurement system can be improved will be made.

1.5 Previous work.

1.5.1 Reciprocating internal combustion engines.

Reciprocating IC engines are widely used to power mobile systems. The main advantages of an IC engine are its high power to weight ratio combined with cheaper cost, fast response and fuel economy when compared to alternative power plants like gas turbines in the same class of power output. These issues are major concerns for

any small to medium sized propulsion systems intended for mobile systems like automobiles and trucks. The basic purpose of the engine is to convert the chemical energy stored in a fuel into mechanical energy. Reciprocating engines have undergone tremendous development since the early 1860's when Otto first patented his four stroke gasoline engine. Much of this development has been aimed at:

- Decreasing the mass of the engine for the given power.
- Improving engine efficiency to get a higher power output.
- Reducing hazardous emissions in the exhaust using controls and aftertreatment.

There is a vast amount of literature regarding internal combustion engines and associated technologies. In surveying the literature for this project the main emphasis was placed on the development of miniature IC engines with applications to model aircraft as well as the development of dynamometers for testing these engines.

1.5.2 Engine testing methods.

Dynamometers have been widely used for evaluating the performance of many kinds of internal combustion engines. Many different types of dynamometer systems are in use today and detailed descriptions of the various types can be found in Judge[15]. While dynamometers make measurements of engine performance at specific loads, a large number of numerical simulations have also been developed to model the engine cycle and predict engine performance. An important advantage of these codes is that they allow the researcher to investigate the effects of specific aspects of the operating physics like friction, heat transfer and the chemistry involved in the combustion process.

1.5.3 Conventional-scale engine performance measurements:

Conventional-scale engine performance measurements have been reported widely in the literature. Advanced techniques like photographic studies of combustion chamber waves[16], in-cylinder pressure measurements[17] and exhaust gas analysis[18] have been used to get detailed information about the combustion process and engine performance at different operating conditions.

Power and torque measurements obtained at different loading conditions show the same general trends for most conventional scale engines. As figure 3 shows, both parameters increase with increasing engine speed and reach a flat peak before decreasing at higher speeds. Engine torque is usually found to peak first followed by a peak in the engine power[19]. Transmission systems in automobiles and other applications are designed to allow the engine to operate in the relatively narrow regimes where it yields maximum power, torque and efficiency.

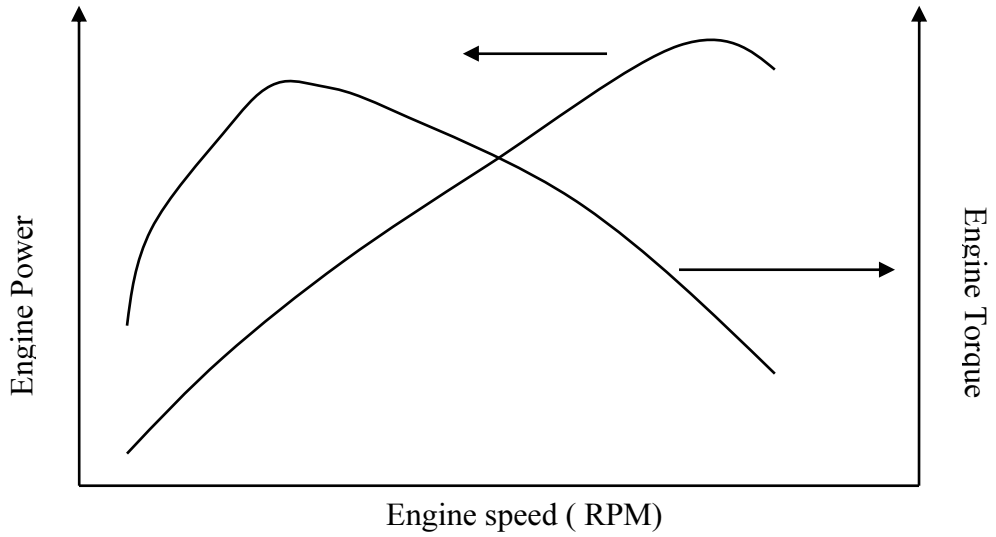

Figure 3 Typical shape of power, torque characteristics of a conventional size 2/4 - stroke engine.

1.5.4 Small engine performance measurements.

Model engine manufacturers usually report peak power for their engines[20] but figure 4 shows that power output varies widely for engines with the same displacement[21] calling the reliability of the performance claims into question. Specific fuel consumption (or efficiency) data is not reported at all because it is of no concern to hobbyists. However it is very important to the designer of any flying vehicle who seeks to maximize range and/or endurance[11].

Hobby magazines have published some reviews of small engine performance over the years[22-27] but the data they provide is incomplete. Usually the evaluation of an engine simply consists of measuring peak RPM with different propellers installed. At most, power output and torque as a function of engine RPM at wide open throttle are reported.

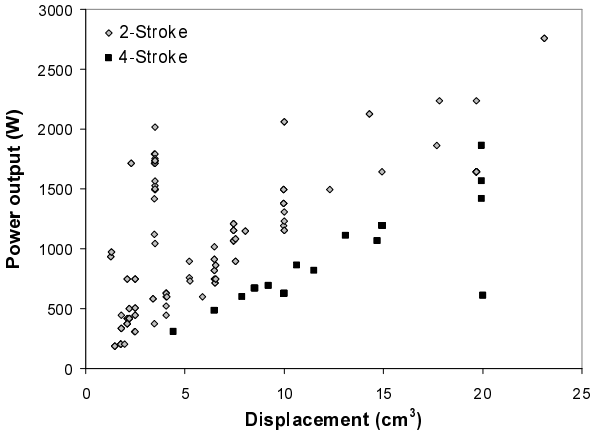

Figure 4 Power output reported by manufacturers as a function of engine displacement[28].

The most extensive investigations of small engine performance have been reported by Gierke in articles that have appeared in various hobby magazines over the past 30 years. He developed a simple dynamometer in 1973 and used it to test a variety of small aircraft engines. Most of his efforts focused on determining the

engine's power curve although specific fuel consumption was reported in a few instances. The present state of the dynamometer is not clear, but his articles document a number of improvements that have been made over the years to assemble a more complete picture of engine performance[29-31]. The engine is mounted on a reaction arm which is held in place using a spring scale. This provides the torque measurement. Speed is measured using a neon tube strobe. The fuel flow rate is measured using a graduated cylinder and a stopwatch. The power output is corrected to standard atmospheric conditions. Loads are applied to the engine using different propellers. Torque and power curves have been generated for a number of engines using this dynamometer[29-31]. A good overview of 2-stroke glow engines are also included in his publication "2-Stroke Glow Engines for R/C Aircraft"[32].

Aside from the efforts of one research group[33-34] and some simple measurements reported by designers of small UAVs[35], there appears to be very little detailed information on the performance of small hobby engines or the testing of small engines in the scientific literature.

1.6 Preliminary analysis of loss mechanisms in IC engines.

The losses in efficiency in reciprocating IC engines can be attributed to factors such as heat transfer, finite combustion time, exhaust blowdown losses, leakage and incomplete combustion. Resistance to unsteady fluid motion through the engine also leads to 'pumping losses' that increase with engine speed.

1.6.1 Frictional losses.

Studies of combustion based micro power systems have shown that frictional and thermal losses scale with the surface to volume ratio of the device[36] which increases as the size of the device is reduced. This results in increased heat losses from the combustion chamber and increased radical extinction (quenching) on the combustor walls, thereby inhibiting good combustion.

Frictional losses also scale with the operating speed of the engine[37]. Since engine speeds tend to be high in model airplane engines (10,000-30,000 rpm), this has an increased effect on frictional losses. Figure 5 shows scaling of surface/volume ratio with engine size. Thermal and frictional losses thus assume significant proportions at the micro-scale. A positive aspect to heat loss is that if correctly channeled it could lead to an improvement in the lifting capabilities of micro-scale airfoils[38]. The basic premise of this technique involves cooling the upper surface of the airfoil while heating the lower surface using waste heat. In case of micro-scale airfoils, the thickness of the thickness of the thermal boundary layer is comparable to the airfoil chord. The heating produces a higher pressure on the underside of the airfoil leading to increased lift.

1.6.2 Incomplete combustion.

Another important parameter affected by engine size as well as operating speed is the residence time of the fuel-air mixture in the combustion chamber. More time is required to burn heavier fuels like hydrocarbon fuels efficiently in comparison with lighter fuels like hydrogen[39]. Figure 6 shows how residence time scales with engine size. In this case, residence time is defined as the average period of time that

the mixture spends in the combustion chamber and is determined from the engine operating speed. At the smallest scales, the residence time approaches the characteristic combustion time for hydrocarbon fuels. As a result we would expect some fuel to exit the combustion chamber without complete combustion leading to a drop in efficiency of the engine. The effect of residence time on the combustion process is quantified using the Damkohler number which is defined as the ratio of the residence time to combustion time. Reducing engine size can reduce the Damkohler number leading to reduced chemical conversion efficiency and lower overall engine efficiency.

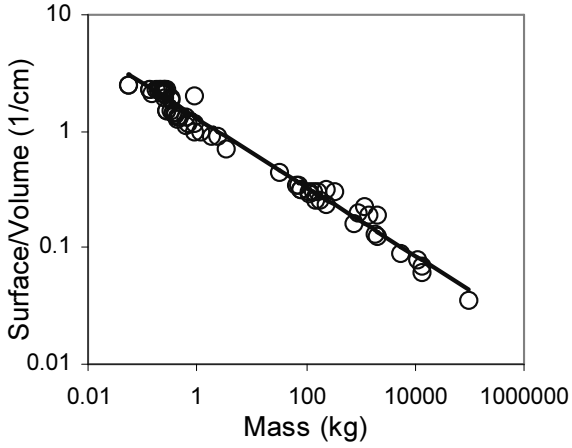

Figure 5 Surface/Volume ratio vs. engine size for a range of piston IC engines.

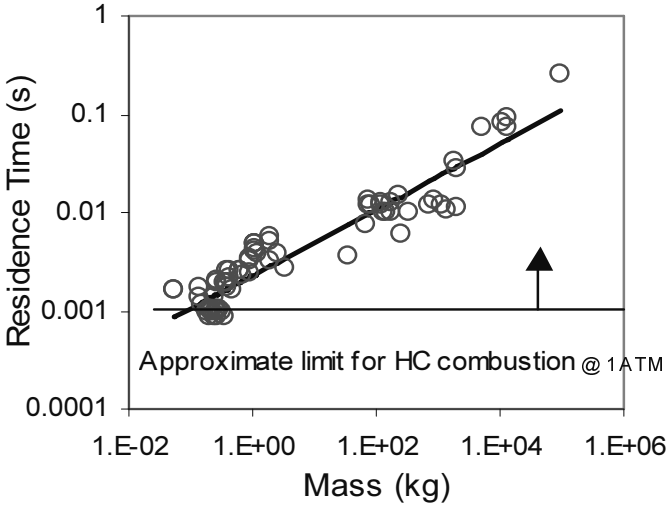

Figure 6 Residence time vs. engine size for a range of piston IC engines.

1.6.3 Heat transfer.

Theoretical analyses based on system-level thermodynamic considerations[18,40] and combustion quenching[41] indicates that the minimum size of a heat engine is on the order of 1 mm^3. Other studies that include the effects of friction and leakage in reciprocating engines arrive at similar conclusions[42]. Since 1 mm^3 is not much smaller than the devices that some micro-engine programs are attempting to construct[43-44] and is only about a factor of 10 smaller than the smallest hobby engines available today, an experimental investigation of how the performance of small engines changes as one approaches this theoretical limit would be very useful.

Such studies also have the advantage of being able to capture the integrated effects of technological factors like engine configuration, timing, machining process, surface friction, heat loss, etc. that are hard to treat collectively through modeling. Thus, it may be possible to determine the relative importance of thermodynamic vs. technological factors on the minimum size of a practical power system.

1.7 Organization of thesis.

This chapter has presented the motivation for the work conducted in this project. It identifies the roles that model airplane engines could play in enabling the development of small UAV's, the need to investigate performance scaling with engine size and the main challenges in the design and operation of engines as propulsion systems for unmanned air vehicles. There is also a brief introduction of the specific measurements to be made, followed by a brief review of the previous research done in this area.

Chapter two gives a brief description of the different engines tested in this work. It explains the fuel delivery, ignition and lubrication systems in the engine. This is followed by a discussion of the fuel used and its relevant properties such as its energy density and its stoichiometric mixture ratio.

Chapter three describes the principle of operation of the dynamometer. It also describes limitations of the current setup and the main challenges associated with the measurements. This is followed by a description of the dynamometer itself with all the associated parts and sensors as well as a description of the data acquisition system used to acquire data from the various sensors. A technique used to reduce vibration on the dynamometer is also discussed along with the techniques used to measure torque, speed and fuel flow rate, the main performance parameters. The methods used to correct measured power to power at standard atmospheric conditions are also described.

Chapter four presents the results of the uncertainty analysis used to estimate error bars for the measured quantities and the performance parameters calculated from the measurements. The uncertainties in the measurements arising from the limitations of the sensors are propagated through the data processing algorithms. The discussion explains the method used to propagate the errors as well as the different kinds of errors considered in the analysis.

Chapter five describes the experimental procedures used to measure engine performance using the dynamometer. Chapter six presents the test results. It begins with a demonstration of the dynamometer's repeatability and a detailed investigation of the performance of a single engine. Less detailed measurements from several other

engines are also reported. These are used to make a preliminary assessment of how engine performance scales with size.

Chapter seven summarizes the major conclusions of this thesis and makes recommendations for future work.

Chapter 2: Engines and Fuels.

2.1 Engine types considered.

Three model single cylinder two-stroke aircraft engines are tested in this work. Single cylinder two-stroke engines were selected because they are well suited for applications in small, low-cost UAV's. Their main advantages over four-stroke engines are:

- Simplicity: Two-stroke engines do not have separate valves for intake and exhaust. Instead they have intake and exhaust ports that are covered and uncovered by the motion of the piston. This makes two-stroke engines lighter, less complex and therefore more reliable.
- Power-to-weight ratio: Two-stroke engines produce a power stroke once every two strokes as opposed to once every four strokes as in a 4-stroke engine. This allows them to achieve a higher power to weight ratio.

Poor thermal efficiency is a drawback of 2-stroke engines; however the advantages of simplicity and power-to-weight ratio make it more a feasible solution for the applications considered here.

2.2 Principle of operation.

Figure 7a shows the steps involved in the version of the two-stroke engine cycle that is commonly used in model aircraft engines. Figure 7b marks the corresponding steps on a pressure-volume diagram of an engine cycle.

- **Intake and compression stroke (parts a & b)**: Starting from bottom dead center (BDC), the piston moves upwards in the cylinder compressing the fresh charge.

At the same time the volume in the crankcase increases. This creates a pressure drop across a rotary valve which is timed to be open during the upstroke and draws in fresh charge (fuel-air mixture) into the crankcase through the intake port. The charge ignites near top dead center (TDC). It is initiated by the catalytic glow plug mounted on the cylinder head. The platinum coated wire in the glow plug creates a hot spot to initiate the combustion process throughout the chamber. This raises the temperature in the combustion chamber well above the ignition temperature and the pressure in the chamber rises rapidly.

- **Exhaust and power stroke (parts c & d)**: The pressure increase associated with the energy release from the fuel drives the piston downwards. The expanding hot gases perform work on the piston during this down stroke. As the piston moves downwards the fresh charge in the crankcase gets compressed because the rotary valve is closed. At some point the piston uncovers the transfer port which allows the fresh charge pressurized in the crankcase to enter the cylinder and force the exhaust gases out through the exhaust port which also becomes uncovered. This technique of removing burnt gases from the cylinder and replacing them by fresh charge is called scavenging and is used in most two-stroke engines.

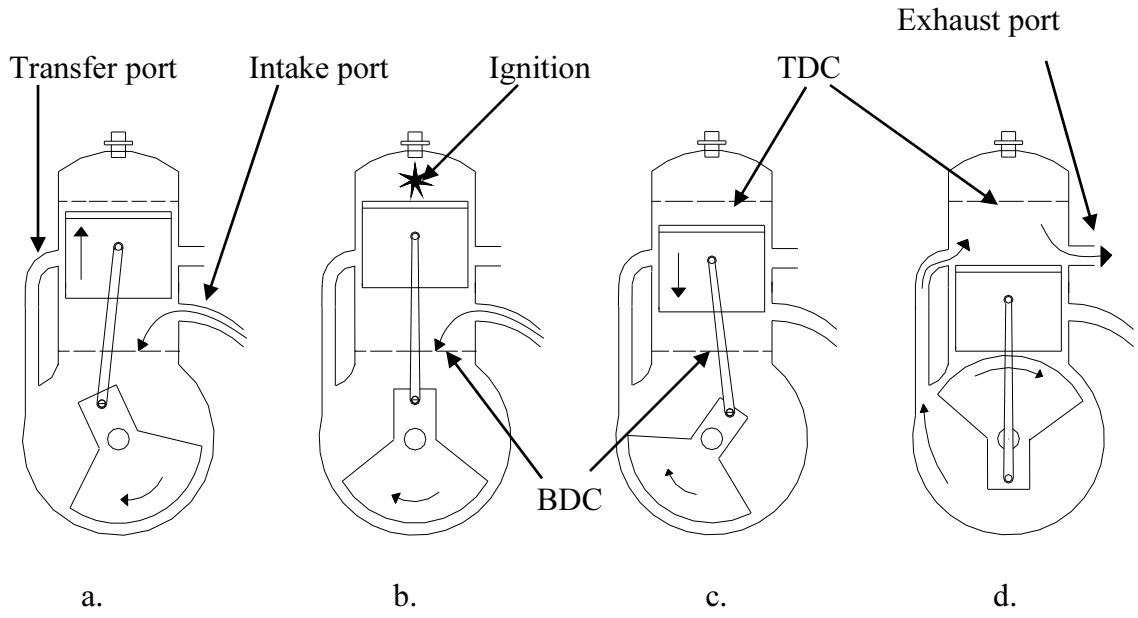

Figure 7a: Steps involved in a two-stroke engine cycle[45].

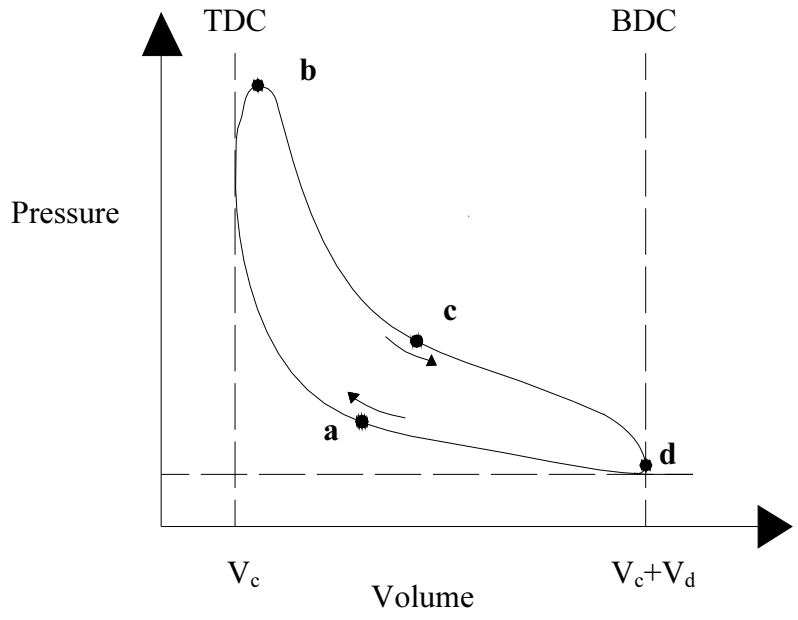

Figure 7b: Steps involved in a two-stroke engine cycle[46].

2.3 Engines considered.

The engines tested on the dynamometer have displacements varying from 1 cc to around 2.5 cc. They weigh from about 75 to 150 grams with the muffler parts

included. The engines are ABC (Aluminum piston, Brass sleeve, Chrome plated) type engines with intake and exhaust porting. Table I gives more detailed specifications for the individual engines including the manufacturer reported performance estimates. Figures 8, 9 & 10 show pictures of the engines tested in this work.

Each engine consists of sub-systems such as the carburetor for fuel air mixing, the intake and exhaust porting, the fuel delivery and lubrication systems and the glow plug which forms the ignition system. These systems, although similar to the corresponding components in automobile engines are adapted to the specific nature of these small engines. These sub-systems are briefly discussed below.

Figure 8: Photograph of the Norvel BigMig Sport engine.

Figure 9: Photograph of the AP Hornet engine.

Figure 10: Photograph of the AP Yellowjacket engine.

Engine	Displacement (cu. cm.)	Weight (gm)	Bore (mm)	Stroke (mm)	Practical speed (rpm)	Manuf. rated power.	Valve Type
Norvel BigMig Sport	1	75	11.17	9.9	4K-22.5K	0.23 KW	Rotary cylinder
AP Hornet	1.475	127.5	12.5	12	4K-18K	0.186 KW	Rotary cylinder
AP Yellow jacket	2.46	150.2	15.5	12	3.5K-18K	N/A	Rotary cylinder

Table I: Comparison of engines tested on the dynamometer.

2.3.1 Carburetion and Induction system.

Carburetors are widely used in most model aircraft engines to achieve fuel-air mixing. While they were used in automobiles for decades, they have since been replaced by electronic fuel injection systems for improved efficiency. However carburetors serve model aircraft engines better due to their simple design. Air enters the engine through the carburetor where a smooth constriction in the air passage (called a venturi) creates a low pressure region that draws fuel into the air stream much like a perfume atomizer.

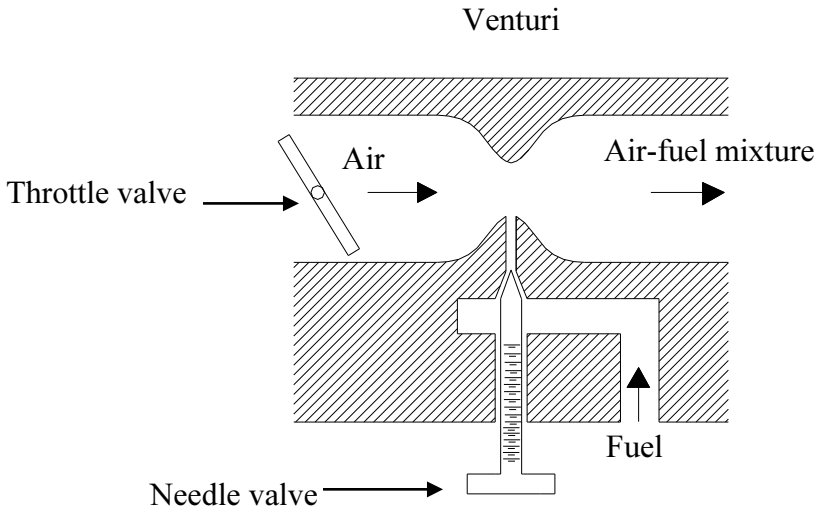

Figure 11: Cross-sectional view of a generic carburetor.

Figure 11 shows a cross-sectional view of a generic carburetor. Fuel flow is metered by a needle valve on the carburetor body. While the needle setting is used to control the mixture ratio, the mixture ratio actually achieved is also affected by operating parameters like engine speed and atmospheric conditions. Air flow through the venturi is controlled by a throttle valve.

Various techniques are used in model aircraft engines for controlling the induction of the fuel-air mixture into the crankcase. The most widely used are rotary valves and reed valves. Both sit between the carburetor and the crankcase. Rotary disk valves are driven by the crankshaft and are designed to be open when the piston is moving upward on the compression stroke. There are two types of rotary valves as illustrated in figures 12 and 13. The first type uses a disk with a cutout that allows flow to pass into the crankcase when the cutout is aligned with the carburetor opening. It is driven by the crank pin. The second type is a cylindrical extension of the crankshaft that passes directly under the port in the crankcase where the

carburetor is attached. This extension also has a cutout in it that, when aligned with the carburetor port, allows fuel-air mixture to pass into the crankcase. The reed valve is an older technology consisting of a set of thin metal or plastic strips held in place by a retaining ring as illustrated in figure 14. The reeds open and close in response to pressure differences applied across them. The cylindrical rotary valve is most common in modern model aircraft engines.

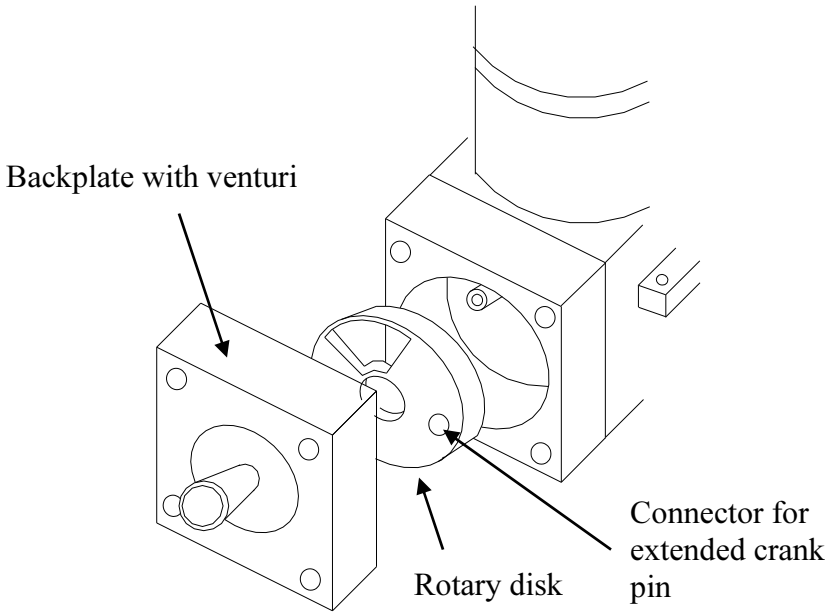

Figure 12 Layout of the rotary disk induction system.

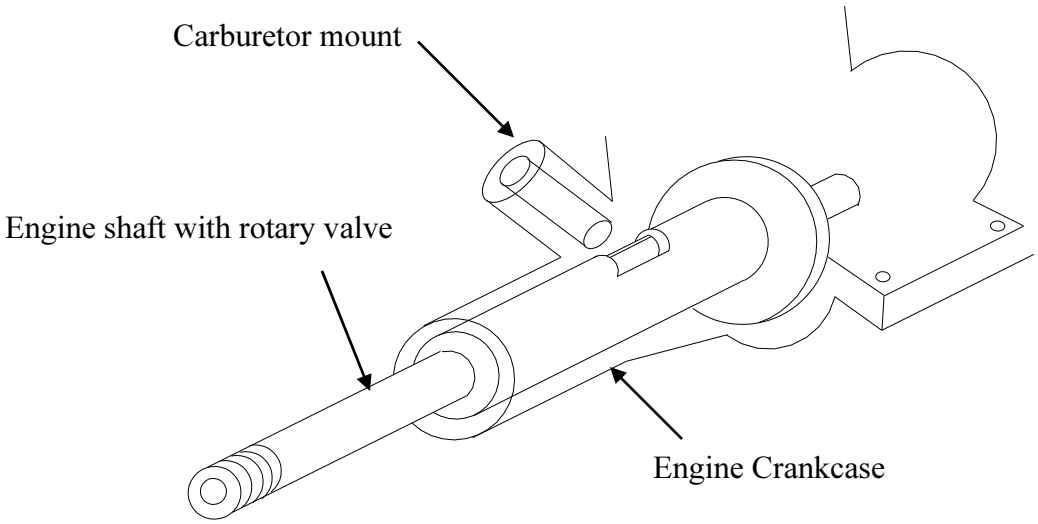

Figure 13 Layout of the rotary valve induction system.

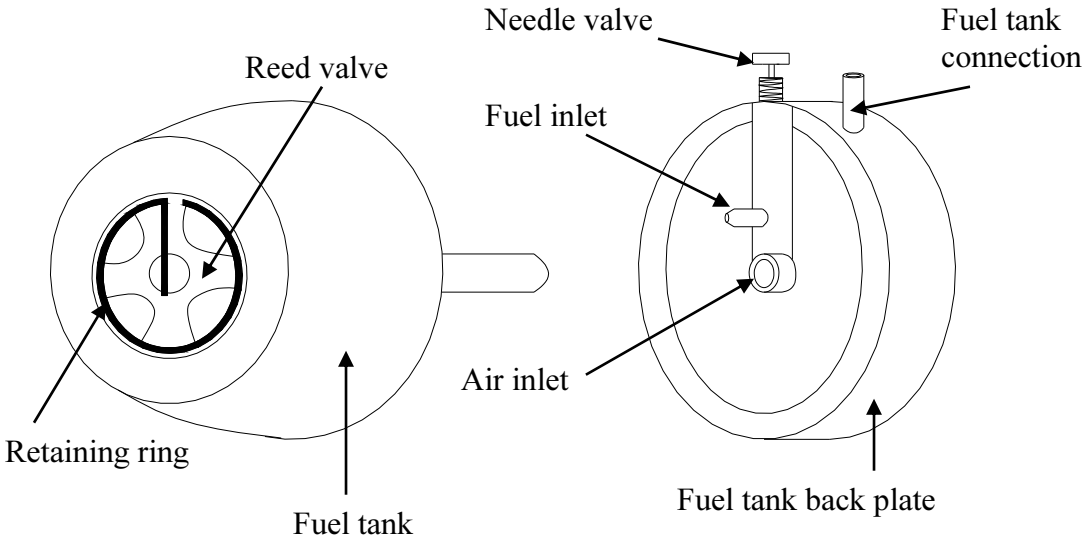

Figure 14 Layout of the reed valve induction system.

2.3.2 Scavenging.

All 2-stroke engines use a scavenging mechanism of one form or another that uses fresh charge to clear the cylinder of burnt exhaust gases. This is important

because the mixing of some part of the burnt gases with the fresh charge and the loss of some of the fresh charge with the burnt gases from the previous cycle that occurs during the scavenging process are two of the main factors affecting efficiency in two-stroke engines. The engines used in this work use an opposed scheme also known as Schneurle porting. Figure 15 shows the basic layout of the system where the flow paths of the transfer ports and the exhaust ports are orthogonal to each other. The transfer ports blow the fresh charge upwards which displaces the exhaust gases downwards and out through the exhaust ports. This is shown in the cross-sectional view of the cylinder presented in figure 16.

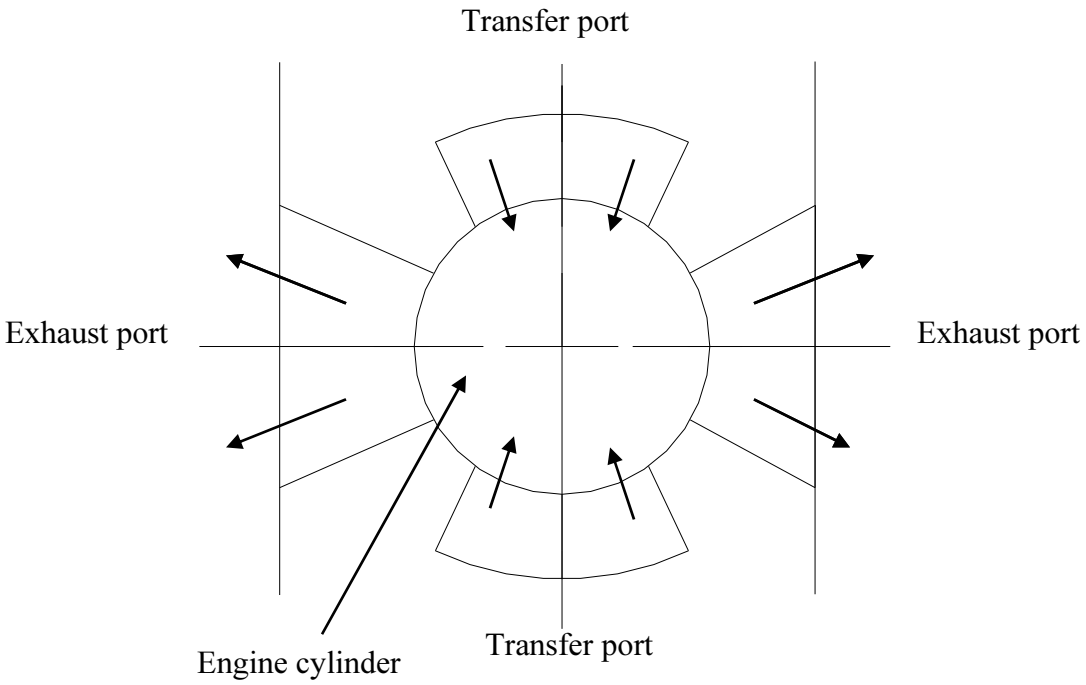

Figure 15 Mixture flow path in the opposed flow/Schneurle ports.

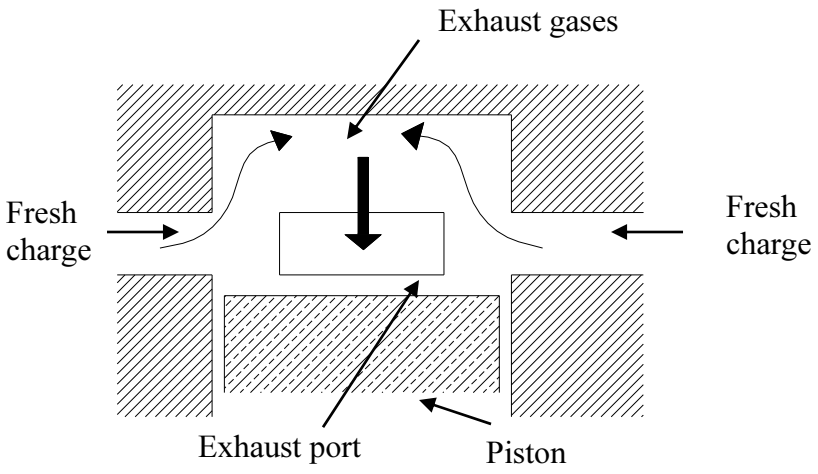

Figure 16: Cross-sectional view of piston and cylinder during scavenging process showing mixture flow paths.

2.3.3 Fuel Delivery.

A common technique used to deliver fuel to the carburetor in many model aircraft engines is to use exhaust gas pressure to pressurize the fuel tank. In such an arrangement, the muffler is equipped with a baffle which creates a high pressure region inside the muffler which is connected to the fuel tank via a flexible tube. The exhaust gas bleed exerts pressure on the fuel in the tank driving it into the carburetor. While this is a simple and light weight scheme it causes the air-fuel ratio to depend on the engine speed in addition to the needle valve setting because the exhaust gas pressure depends on engine rpm. The fuel pressure can also be changed by placing the tank at different elevations relative to the engine because of hydrostatic pressure. In the experiments done here, however, the fuel tank was always maintained at approximately the same elevation as the engine.

2.3.4 Ignition.

Combustion of the fuel-air mixture is initiated by a glow plug mounted on the cylinder head. This glow plug consists of a threaded housing, an insulated electrode and a coiled resistive platinum wire connecting the electrode to the housing. The wire acts as a catalytic initiator for combustion. Figure 17 shows a picture of a commonly used glow plug. The wire must be heated in order to initiate combustion and this is accomplished in one of two ways:

- During startup it is heated by electric current (600 mA) supplied by a 12 V battery.
- After startup, the catalyst wire is kept hot by the heat released during the combustion process.

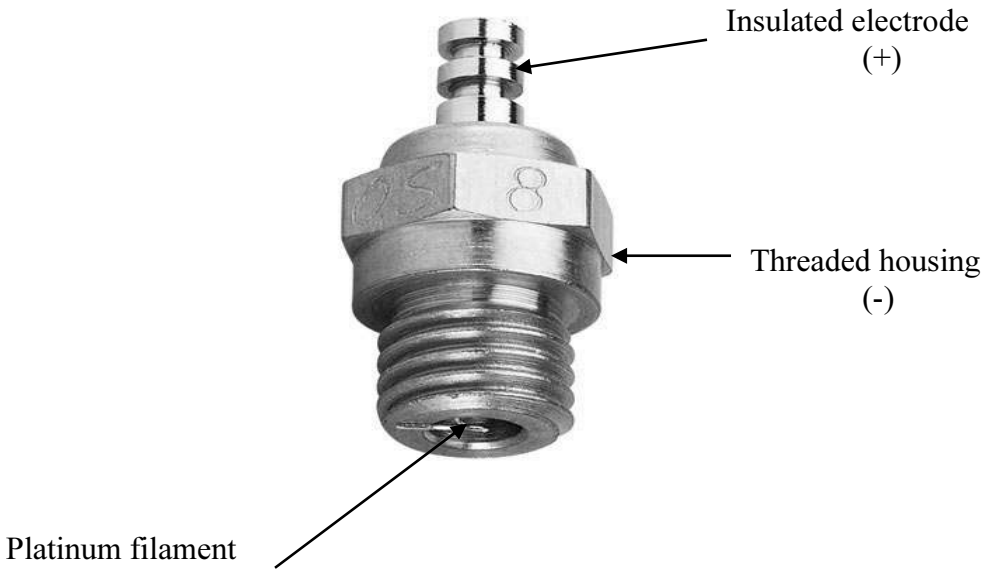

Figure17 Picture of an OS#8 glow plug.

The condition of the glow plug can have a strong effect on engine performance. However it acts as a purely passive initiator and hence cannot be used like a spark plug in automobile engines to change ignition timing. Therefore, alternative methods for controlling ignition timing have to be found. A crude alternative is to change the compression ratio by using spacers to increase or decrease the volume of the combustion chamber. However this cannot be done in real time and another approach would be required to achieve true timing control.

2.3.5 Lubrication and Cooling.

Lubrication is an important issue in small scale engines. Frictional losses scale with surface to volume ratio which means that they are very important in small engines. However separate lubrication systems are usually not feasible due to limitations on complexity of construction and weight. Therefore nearly all model airplane engines mix the lubricant with the fuel. Typically oil accounts for 10-20% of the fuel mixture and is either synthetic or castor-oil based. Fuel combustion is discussed more extensively in the next section but one important fuel property not related to combustion is the fuel's ability to absorb heat during the vaporization process thereby assisting in engine cooling. However the main engine cooling mechanism remains the convective heat transfer from the finned cylinder head to the surrounding air flow from the propeller. Since the engine is operated without a propeller, an external blower supplies cooling air when the engine is on the dynamometer.

2.4 Fuels.

The engines used in this work are designed to operate on 'glow fuel' which is a mixture of methanol (CH_3OH), nitromethane (CH_3NO_2), and castor oil ($C_{18}H_{34}O_3$). Different fuel mixtures are commercially available. Mixtures with larger amounts of nitromethane and lesser amounts of castor oil generally produce more power but at the expense of engine operating life. This work uses a relatively conservative 70% methanol, 10% nitromethane, 20% castor oil mixture. Because fuel evaporation is important for engine cooling, the high latent heat of methanol is another reason for its choice as a model engine fuel. Ideally, the oil component of the fuel would not contribute to the heating value of the overall fuel mixture but a significant fraction of the oil does appear to burn during engine operation. This will be discussed later.

The heating value of the mixture was measured by a commercial fuel testing laboratory using standard procedures[47] and found to be 21.82 MJ/kg. Table II gives the composition and density of the fuel mixture as well as an estimate of the mixture's overall heating value based on the heating values of the individual constituents. We were unable to find a reliable reference for the heating value of castor oil, so the value of 29.9 MJ/kg was chosen to match the measured heating value of the mixture. The density of the fuel mixture is given by:

$$\rho_{mix} = \rho_m \chi_m + \rho_{nm} \chi_{nm} + \rho_o \chi_o \tag{2}$$

where χ_m, χ_{nm}, and χ_o, are the volume fractions of methanol, nitromethane and castor oil in the fuel. Similarly ρ_m, ρ_{nm}, and ρ_o are the densities of the various components. The heating value of the mixture is given by:

$$Q_{r,mix} = \rho_m Q_{r,m} \chi_m + \rho_{nm} Q_{r,nm} \chi_{nm} + \rho_o Q_{r,o} \chi_o \tag{3}$$

The complete calculation for the stoichiometric fuel/air ratio of a sample fuel mixture is given in Appendix A. For the fuel mixture used in the experiments, the stoichiometric fuel/air ratio was found to be 0.152 (or 0.227 on a mass-basis) assuming that the castor oil is inert i.e. none of it burns. This lowers the effective heating value of the fuel mixture to 15.2kJ/gm. However we use the experimentally determined heating value of 21.82 kJ/gm to compute the overall efficiency of the engine because the unburned lubricant represents energy that is wasted and we have no means to determine how much of the lubricant may have reacted. Nevertheless, the degree to which the castor oil reacts has a strong impact on the operating equivalence ratio. For example, if 100% reacts, the stoichiometric fuel/air ratio becomes 0.096 (or 0.144 on a mass basis).

Component	χ	ρ	Q_r
CH_3OH	0.7	0.81	21.12
CH_3NO_2	0.1	1.13	11.6
Castor Oil	0.2	0.96	44.0
Mixture	1.0	0.875	21.8
		g/cm^3	kJ/g

Table II Properties of glow fuel constituents and overall properties of the mixture.

Table II shows that the energy density of nitromethane is lower than that of methanol. Therefore adding nitromethane to the fuel mixture actually reduces its energy density. However it is also well known that adding nitromethane to the fuel can increase the engine's power output by up to 20%[48]. While this may seem

contradictory, the reason for this is that nitromethane mixtures require less oxygen to burn because the nitromethane molecule already has two oxygen atoms incorporated into its chemical structure. This means that fewer moles of air are required to burn one mole of fuel and that more moles of fuel can be burnt in one stroke. This more than compensates for the lower energy density of the fuel.

Figure 18a shows constant energy contours for different mixtures of the three fuel components assuming that the oil does not burn. The individual component mole fractions can be read along the straight lines on the tri-axis. Any point formed by the intersection of the three axes corresponds to a particular mixture combination. The mole fraction of the components along each axes go from 0 to 1. Hence the top of the triangle would correspond to the point where the mixture is 100% nitromethane, the lower left vertex corresponds to 100% methanol and the lower right vertex corresponds to 100% oil. Energy contours are plotted in grayscale with the energy content decreasing from light to dark. Figure 18b shows the stoichiometric fuel/air mixture ratio as a function of the mole fraction of nitromethane in a fixed volume of the fuel mixture. Figure 18c shows the results of a chemical equilibrium calculation (GASEQ) where heat released by the combustion of a fixed volume of fuel with different quantities of nitromethane is determined. The fuel/air ratio of the mixture is kept constant and the oil component is assumed to remain unburnt. As the figure shows, the addition of nitromethane reduces the effective equivalence ratio of the fuel rich mixture. This results in an increase in the net heat release.

While adding nitromethane can also be used to control ignition timing because nitromethane has a lower ignition temperature compared to methanol, adding too

much nitromethane causes knocking (i.e inhomogenous combustion). Since more energy is released per stroke, it also increases engine temperature and can dramatically shorten engine life.

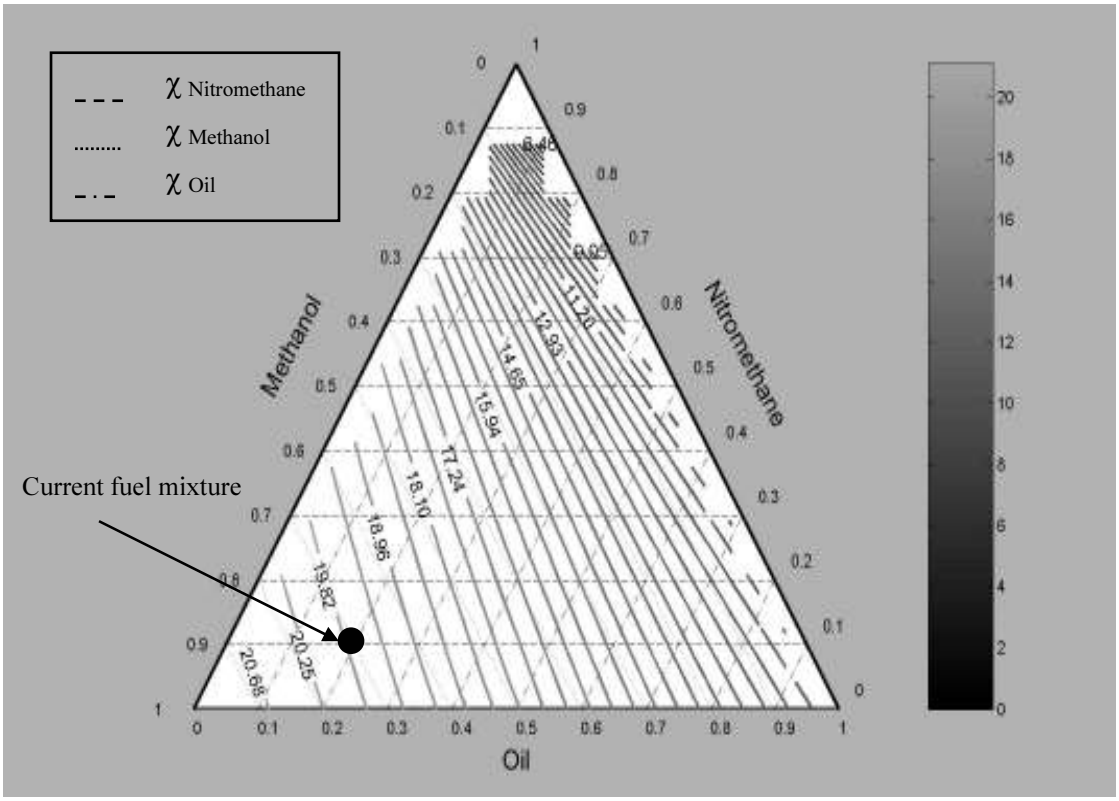

Figure 18a Constant energy contour plot for variable fuel mixtures.

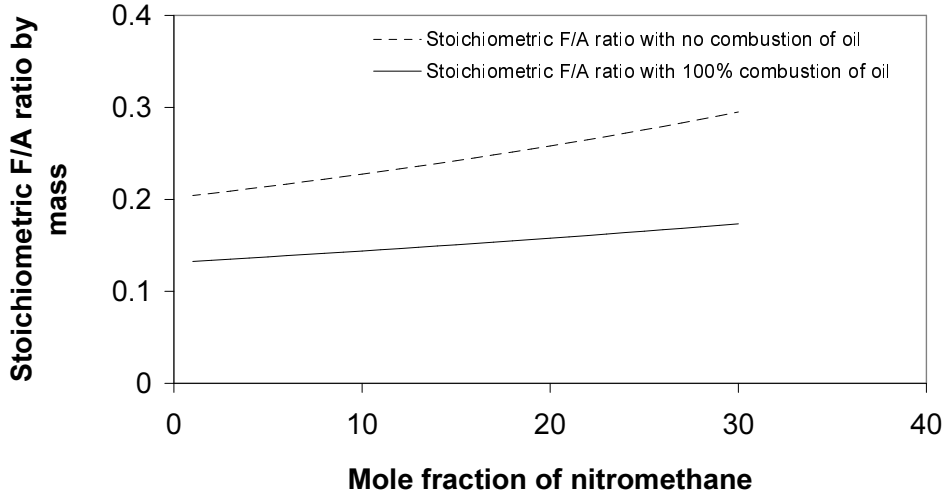

Figure 18b Stoichiometric F/A ratio as a function of nitromethane mole fraction.

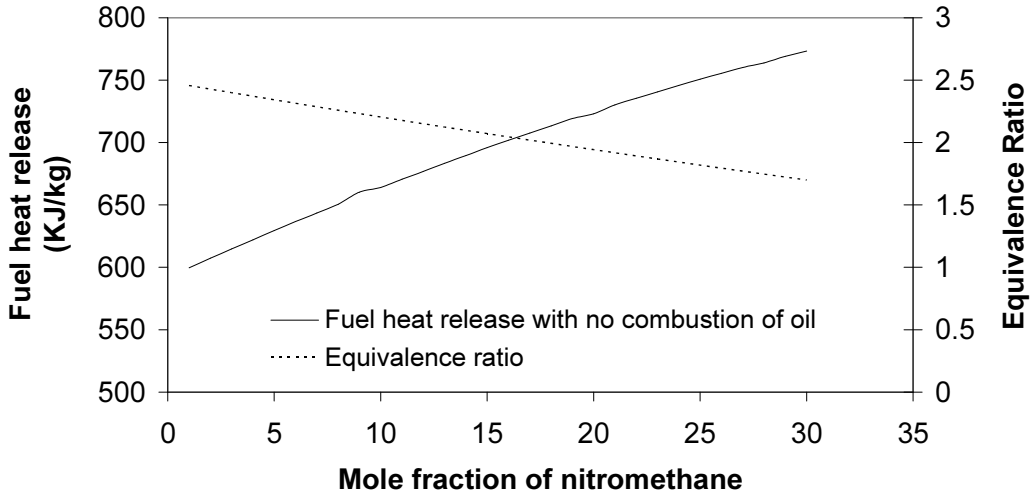

Figure 18c Heat release and equivalence ratio as a function of nitromethane mole fraction.

Chapter 3: Experimental Apparatus.

3.1 Types of Dynamometers.

Dynamometers are devices for measuring the torque and speed of a rotating machine. They can be broadly classified into absorption and transmission types. Absorption dynamometers absorb the power produced by the engine while transmission dynamometers merely transmit the power through to other power consuming machinery. Absorption dynamometers are classified according to the manner in which the absorbed energy is dissipated.

- Friction dynamometers: Absorbed energy is converted to heat and is dissipated using frictional devices like mechanical brakes.
- Hydraulic and air dynamometers: Absorbed energy is converted to heat and dissipated via friction forces associated with the motion of a working fluid which may be water or air.
- Magnetic and eddy current dynamometers: Absorbed energy is dissipated and converted to heat via joule heating.

Transmission dynamometers are useful in circumstances where the engine is to be tested under natural working conditions like in an airplane or in an automobile. These are less accurate than absorption type dynamometers and are used less often[49]. The dynamometer used in this work is an absorption type dynamometer with a magnetic hysteresis brake for energy absorption/load control.

Figure 19 is a schematic diagram of the dynamometer system illustrating the various components. The engine to be tested is mounted in a cradle that rotates about

an axis coincident with the engine's axis of rotation. The cradle is prevented from rotating by a single load cell that anchors it to the cradle support.

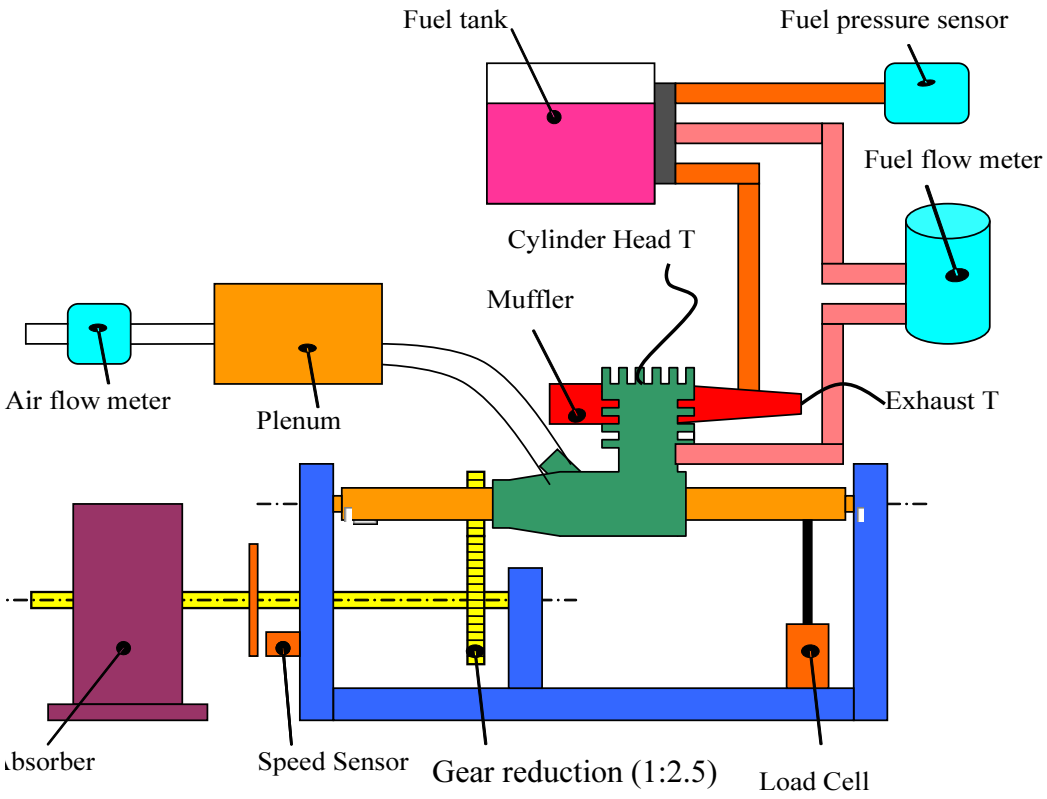

Figure 19: Schematic diagram of dynamometer showing the engine installed on the cradle and the important sensors.

3.2 Torque measurement principle.

The engine torque is measured using the torque reaction method[50] which is particularly well suited for small engine applications. It involves mounting the engine on a freely rotating cradle and measuring the torque required to hold the engine in place using a standard load cell. The applied load causes the engine to produce a reaction torque by Newton's third law of action and reaction. The product of the torque with the engine speed gives the output power. An alternate approach would be to mount the engine rigidly and measure the reaction torque at the absorber. This has

the disadvantage, however that losses associated with the transmission system consisting of gears or belts must be estimated. Since the engines being tested here are relatively small, the torques they produce are small and the measurements would be particularly sensitive to estimates of transmission losses. These losses do not affect the reaction type dynamometer and thus it is best suited for testing small engines and is the one we use here.

3.3 Hysteresis brake.

The absorber used in this application is a Magtrol HB series hysteresis brake capable of producing 840 oz-in. of torque at its rated current of 160 mA. The maximum rated speed of the brake is 6000 rpm. Figure 20 is a cross-sectional view of the brake illustrating the important components. The brake consists of a reticulated pole structure and a rotor/shaft assembly with high magnetic permeability. The two parts are separated by an air gap. In the absence of a current in the field coil, no force is exerted on the rotor/shaft assembly and it is free to spin. When a current is applied to the windings, a magnetic field is created across the air gap and through the rotor. The motion of the rotor in the magnetic field produces an eddy current in the rotor and a braking torque associated with the resistance to current flow in the rotor. The hysteresis brake has the following advantages over devices using shear or frictional forces to achieve the same effect:

- Infinitely variable loads – Torque is adjusted by varying current flow through the coil. The minimum torque is equal to the bearing frictional drag while the maximum torque is produced at the rated current and is independent of speed.
- Smooth and quiet operation.

- Low wear – The only components of the brake exposed to wear are the shaft bearings. Other devices contain components like pulleys, ropes and other rotating machinery, all of which are subjected to wear.
- Applied torque is independent of operating speed- The applied torque is solely a function of the current passing through the coils and is hence independent of operating speed. This greatly facilitates engine control.

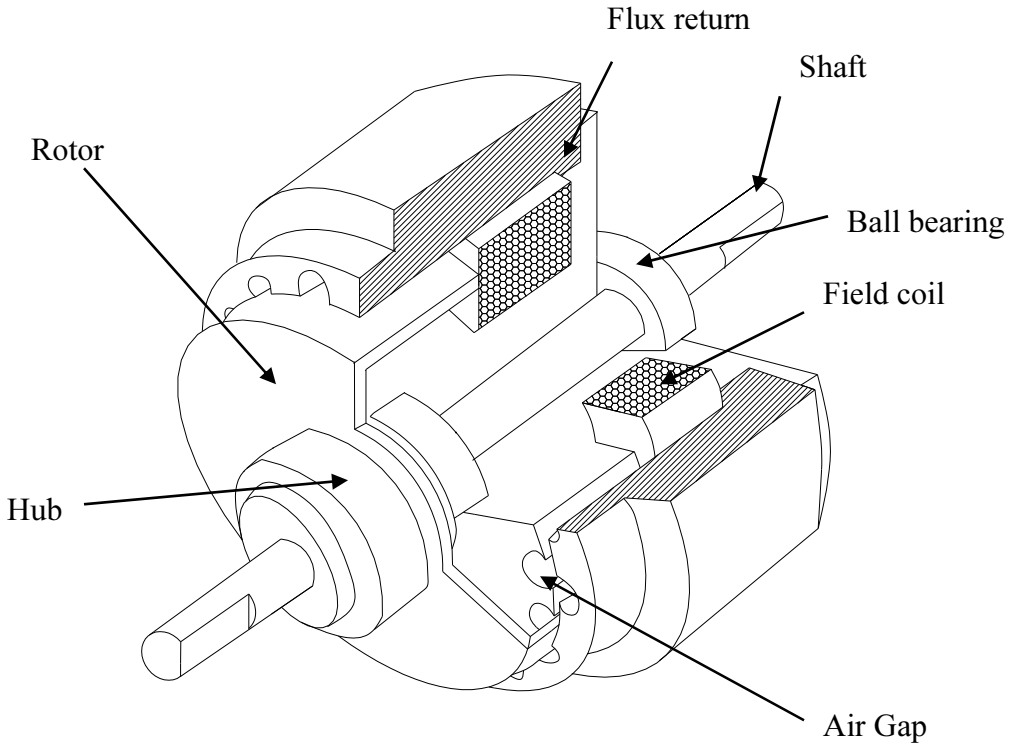

Figure 20 Cut-out of the hysteresis brake showing the important parts[51].

3.4 Dynamometer operation.

An operating point of the engine-dynamometer system corresponds to a situation where the power produced by the engine exactly equals the power consumed by the absorber. The operating point can be visualized as the intersection of the characteristic power-speed curve of the engine with that of the absorber as illustrated

in figure 21. Whether or not the operating point is stable depends upon the respective shapes of the engine and absorber power curves. In this work, the power curve of the absorber is a straight line with slope proportional to the field current (other absorbers like propellers and water brakes have non-linear characteristics). The power curve of the engine is what we would like to determine and has the general shape of an inverted parabola. Point A is a stable operating point because small disturbances in speed create forces that tend to push the system back to its original speed: An increase in speed causes the engine to decelerate because the brake is consuming more power than the engine is producing while decrease in speed causes the engine to accelerate because the engine is producing more power than the brake is consuming. In contrast, point C is not stable because a small increase in speed would allow the engine to accelerate away from point C and a small decrease in speed would allow the engine to decelerate away from point C. Point B, where the brake characteristic is tangent to the engine power curve marks the passive stability limit of the system.

There are several ways to determine the power curve of the engine but one way is to fix the throttle and mixture settings and adjust the current to the hysteresis brake so as to sweep the brake characteristic (and point A) along the power curve of the engine. Torque and speed are measured at various points along this curve to determine power. This is the approach taken here. However, this approach breaks down for points to the left of B where the dynamometer is not naturally stable and a separate control system for the dynamometer is required to measure engine performance in this region. The dynamometer system described in this thesis does not have a control system and therefore only measurements corresponding to operating

points to the right of point B are reported. Since point B corresponds to engine speeds that are much smaller than those envisioned for operation of the engines considered here, this truncation of the power curve should not pose a significant problem.

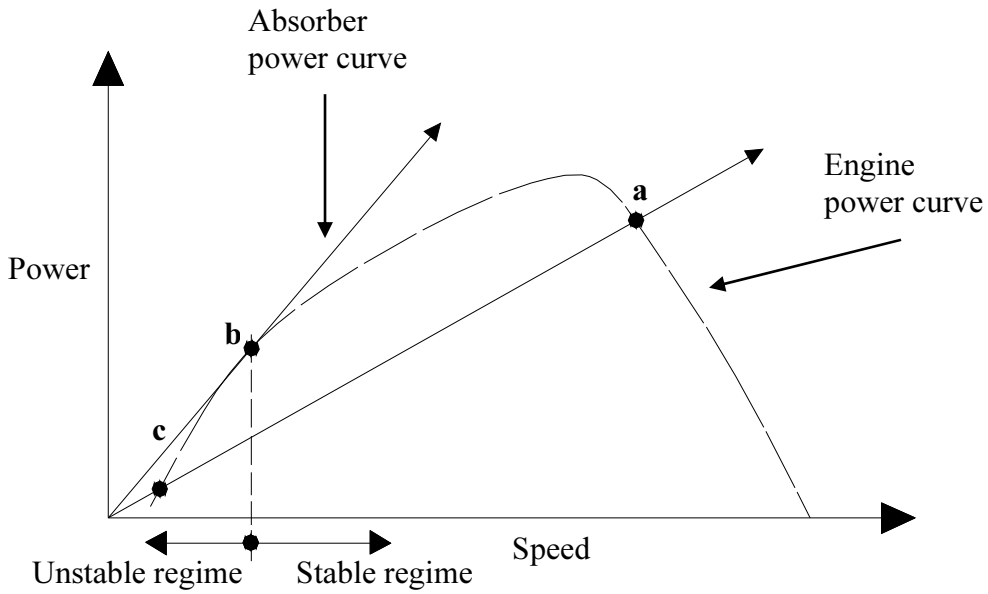

Figure 21 Stable and unstable operating regimes of a model engine.

The engine can still be operated in a controlled or an uncontrolled mode in the stable operating regime. In the uncontrolled mode position and mixture setting are held fixed and a torque curve is obtained by sweeping through different loads. In the controlled mode, the engine speed is held constant by varying the load as the fuel-air mixture ratio is adjusted. This enables us to explore the effect of fuel-air mixture on power output to determine the optimum mixture settings for different operating conditions like maximum power and best economy. Both control modes are used to characterize the performance of the engine.

3.5 Challenges.

There are several factors that complicate performance measurements in these small engines. First, operating speeds are relatively high (8000-20,000 rpm) which means that high speed transmissions are required to remain to within the 8000 rpm limit of the hysteresis brakes. Secondly, the range of fuel flow rates is not accessible by most off-the-shelf liquid flow meters. This is further complicated by the fact that the pressure driving the fuel flow in the engines being considered here ranges from 3 to 7 KPa so pressure losses through the flow meter need to be small (<0.03 KPa). Third, engine torque levels are relatively low but ambient noise (vibration) levels are high because all of these small engines are single cylinder designs. As a result, care must be taken to damp the strong 1/rev and 1/2rev disturbances so as to prevent them from exciting resonant modes of the measurement system. At best, failure to control vibration degrades the accuracy of the torque measurement by raising the background noise around a small torque signal. At worst, it can destroy the torque/force sensor. Finally, the dynamometer system must be flexible enough to accommodate a wide range of engines with minimal mechanical modifications.

3.6 Dynamometer.

Figure 22 is a photograph of the dynamometer illustrating the major components. The engine to be tested is mounted in a cradle that is supported on precision low-breakaway torque bearings (<0.02 oz-in) about an axis coincident with the engine's axis of rotation. The cradle is prevented from rotating by a load cell that anchors it to the cradle support. The absorber is connected to the engine through a gear system and provides a continuously variable load to the engine. As the load is

applied, the engine reacts against the cradle causing a load to be exerted on the load cell. The product of the load cell force and the moment arm length gives the engine torque. The load cell is a Sensotek model 31 with a full-scale capacity of 5 lb. Additional information about the cell is presented in table III.

As mentioned previously one advantage of this torque measurement scheme is that no accounting needs to be made for losses in the powertrain. Another advantage is that using a load cell and adjustable moment arm as opposed to a dedicated torque sensor allows the sensitivity of the instrument to be adjusted for different engines by attaching the load cell to the moment arm at different radial locations. This also means that a single load cell can be used to test a relatively wide range of engines.

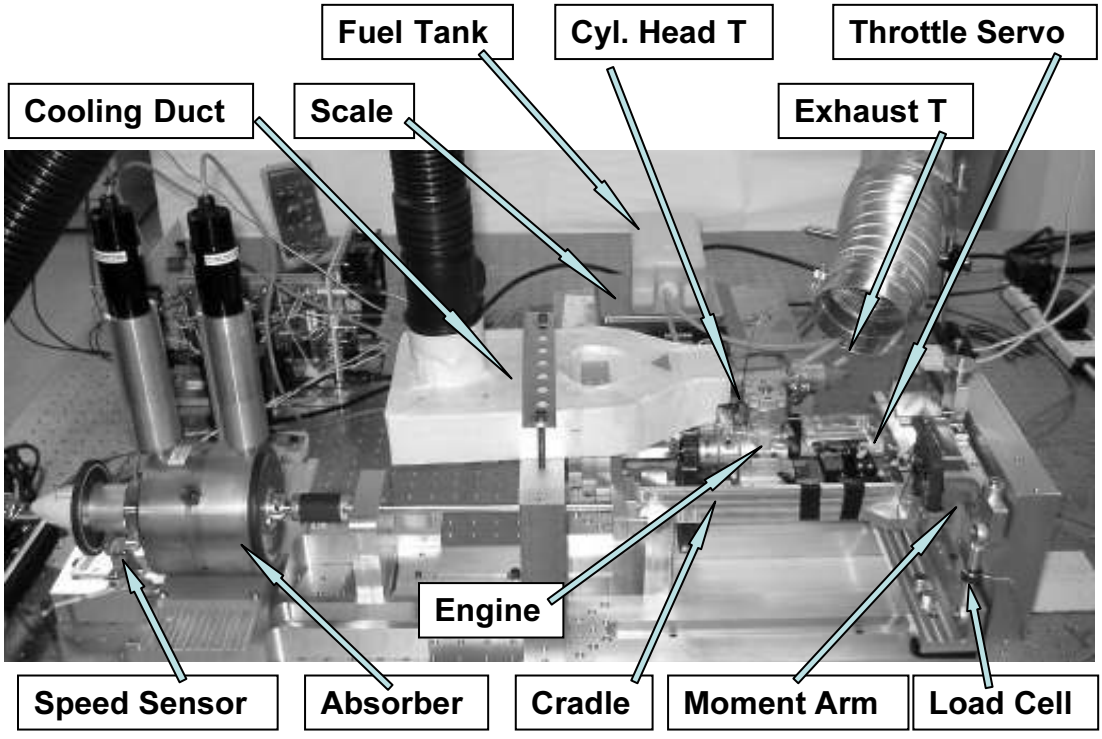

Figure 22 Photograph of dynamometer system showing the important components.

The engine to be tested is mounted on the cradle and secured using allen head cap screws. The throttle is controlled remotely using a Futaba servo, FM receiver, and

battery all attached to the cradle. This enables throttle adjustments to be made without touching the engine and influencing the torque measurements. Thermocouples attached to the engine measure cylinder head and exhaust gas temperatures. While both thermocouples are terminated on the cradle support, the forces exerted by their tips have negligible impacts on the torque measurement. The fuel flow measurement in this case is done using a scale with a voltage output. Two flexible hoses connect the fuel tank to the engine on the cradle. One delivers the fuel to the needle valve inlet. The other extends from a fitting on the muffler back to the fuel tank to pressurize it. As explained further on, fuel flow for larger engines is measured using a flow meter and not the scale system. This is because the flow meter improves measurement accuracy. However it introduces a pressure drop which affects fuel flow adversely in smaller engines with low driving pressure. Fuel pressure is measured by a pressure sensor. The forces exerted by the hoses on the cradle do impact the torque measurement but these are accounted for by calibrations performed before and after every run.

An air flow sensor measures air intake. Since the flow sensor only works properly under steady flow conditions, a plenum is placed between the sensor and the carburetor inlet in order to damp out fluctuations in the flow of air. These fluctuations are a strong and inherent feature of any reciprocating engine. A flexible tube connects the plenum to the carburetor in order to minimize the impact on the torque measurements. Parasitic torques associated with the tube are also accounted for during the calibration of the cradle. The volume of the plenum is considerably larger (3000 times) than the displacement of the engine being tested in order to provide

maximum damping of flow oscillations with minimum pressure loss. The length of the tube is also kept as short as possible in order to minimize pressure loss. The total pressure loss through the plenum and tube is less than 0.01% at the maximum flow rate. This is calculated using the dimensions of the connecting tube and assuming fully developed flow of air in the tube with a parabolic velocity profile. The Reynolds number for the flow lies in the laminar regime and allows the calculation of the friction factor from which the head loss is determined. The head loss in the plenum is assumed to be 5 times as much as the head loss in the tube.

The maximum operating speed of the absorber is 8000 RPM. Since the maximum operating speed of the engine being tested is generally higher, a geared transmission is used to connect the brake to the engine. A DC source supplies current to the brake and can be controlled from a panel-mounted potentiometer or a 0-5V analog signal. The brake is rated to dissipate up to 800W of power without forced air cooling. More power can be dissipated on an intermittent basis or if cooling air is provided. Two infrared thermocouples monitor the temperatures of the brake drums. So far, it has not been necessary to actively cool the brakes.

The engine speed is that reported by the speed sensor attached to the hysteresis brake multiplied by the gear ratio of the transmission. A model aircraft propeller nose cone attached to the end of the absorber shaft permits the engine to be started using a conventional model aircraft starter. Cooling air for the engine is provided by a specially constructed duct that directs air from a blower around the moving parts of the cradle and directly across the cylinder head. The engine will overheat rapidly without the cooling air.

3.7 Sensors and Measurements.

3.7.1 Torque Measurement.

Figure 23 is a vector plot showing the relationship between the torques and forces acting on the cradle. The x and y axes intersect at the center of rotation of the cradle and the z axis extends along the cradle's axis of rotation.

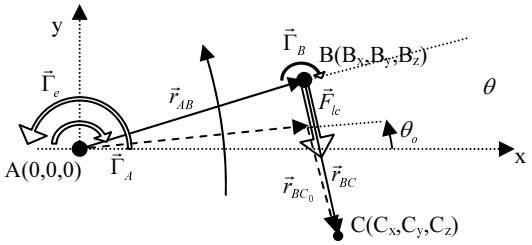

Figure 23 Vector diagram showing the forces acting on the torque-measuring cradle and the mechanical constraints imposed on the cradle/load cell system.

A force balance on the cradle leads to the following expression for the torque $\vec{\Gamma}_e$ exerted by the engine on the cradle

$$\vec{\Gamma}_e = \vec{\Gamma}_A + \vec{\Gamma}_B - \vec{r}_{AB} \times \vec{F}_{lc} \tag{4}$$

where $\vec{F}_{lc}$ is the vector associated with the force applied by the load cell on the cradle. $\vec{\Gamma}_A$ and $\vec{\Gamma}_B$ are respectively the parasitic torques associated with the cradle bearing and the load cell attachment points. The moment arm is represented by $\vec{r}_{AB}$ which extends from the cradle's center of rotation (A) to the load cell attachment point (B). The cradle is constrained by $\vec{F}_{lc}$ which acts along the load cell axis $\vec{r}_{BC}$. The objective is to use the measurements of $\left|\vec{F}_{lc}\right|$ made by the load cell to determine the torque produced by the engine. The difficulty is that the load cell deforms under the influence of the load allowing the cradle to deflect through an angle $\theta - \theta_o$. While

not accounting for the deflection is fine for the dynamometer system described here, other systems are equipped with an elastomeric element between the load cell and the cradle to help damp vibration. In these systems, the deflection is relatively large and must be accounted for when computing $\vec{F}_{lc}$ in equation 1. Accordingly, we will go through the procedure for solving the more challenging problem involving large deflections.

Determining $\vec{F}_{lc}$ begins by recognizing that:

$$\vec{F}_{lc} = \left|\vec{F}_{lc}\right| \frac{\vec{r}_{BC}}{\left|\vec{r}_{BC}\right|} \tag{5}$$

Since $\left|\vec{F}_{lc}\right|$ is known (via the measurement), the challenge is to find $\vec{r}_{BC}$. This is accomplished as follows. First, note that $\vec{r}_{BC}$ is constrained by the center of rotation of the cradle (A) and the load cell anchor point (C) which are fixed:

$$\vec{r}_{BC} = \vec{r}_{AC} - \vec{r}_{AB} \tag{6}$$

Second, $\vec{r}_{AB}$ is constrained to the x-y plane, so it can be written in terms of a single independent variable θ_o, the angle of the cradle,

$$\vec{r}_{AB} = R\cos\theta_o \hat{i} + R\sin\theta \hat{j}0_o + \hat{k} \tag{7}$$

In this equation $\hat{i}$, $\hat{j}$ and $\hat{k}$ are unit vectors associated with the x, y and z directions respectively and *R* is the length of the moment arm. Equations 3 and 4 lead to similar expressions for the fixed quantities $\vec{r}_{BC\,0}$ and $\vec{r}_{AB_0}$ that are associated with the initial (unloaded) position of the cradle.

$$\vec{r}_{BC_0} = \vec{r}_{AC} - \vec{r}_{AB_0} \tag{8}$$

$$\vec{r}_{AB0} = R\cos\theta_0\hat{i} + R\sin\theta_0\hat{j} + 0\hat{k} \tag{9}$$

$\left|\vec{r}_{BC}\right|$ is found using Hooke's law

$$\left|\vec{F}_{lc}\right| = k_{lc}\left(\left|\vec{r}_{BC}\right| - \left|\vec{r}_{BC_0}\right|\right) \tag{10}$$

where k_{lc} is the stiffness of the load cell and $\vec{r}_{BC\,0}$ is known and constant. Equations 5 through 8 can be solved for the cradle deflection angle θ as a function of the magnitude of the load cell reading $\left|\vec{F}_{lc}\right|$. Once the deflection angle is known, it is used to calculate $\vec{r}_{AB}$, $\vec{r}_{BC}$ and finally $\vec{F}_{lc}$ via equations 6, 5 and 3 respectively.

Table III Parameter values for torque measurement system.

Parameter	Value	Uncertainty	Unit
R	0.635 – 13.3	+/- 0.005	cm
$\left\|\vec{F}_{lc}\right\|$	0 – 22.25	+/- 0.21% FS	N
δ_{max}	0.012-0.05	+/- 0.025	mm
k_{lc}	174880-437200	+/- 218600	N/m
θ_0	0	+/- 5	Deg
C_x	0.6 – 13.3	+/- 0.005	cm
C_y	-10.16	+/- 0.005	cm
C_z	0	+/- 0.0012	m
$\vec{\Gamma}_A \circ \hat{k}$	1.4e-3	+/- 1.4e-3	N-m
$\vec{\Gamma}_B \circ \hat{k}$	< 1.4e-3	+/- 1.4e-3	N-m
I_e	>0.0142	+/- 0.0142	N-m^2
I_c	>0.0854	+/- 0.0142	N-m^2
m	11.93	+/-0.1133	N
r	0.1	+/-0.0002	m

Table III Parameter values for torque measurement system.

Table III shows the values of the quantities referred to in equations 3 through 9 for the dynamometer system. The moment arm length R is adjustable through nine increments from 0.25 in to 5.75 in. The load cell attachment point C is also adjustable through the same nine increments and is set so that $C_x = R$. The stiffness

of the load cell k_{lc} is estimated using the maximum rated force of the load cell and the maximum deflection of the load cell via:

$$k_{lc} = \left|\vec{F}_{lc}\right|_{\max} \Big/ \delta_{\max} \tag{11}$$

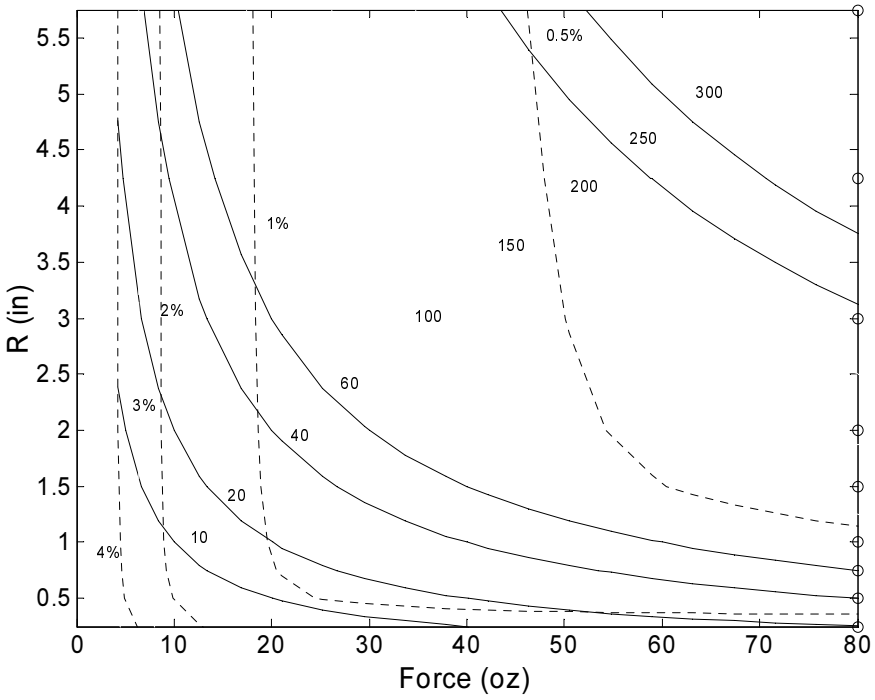

Figure 24 Contours of torque (oz-in) and uncertainty in torque (%, dotted contours) as a function of load cell force and moment arm length R.

While the uncertainty in k_{lc} is relatively large because of the relatively large range of possible load cell deflections δ_{max}, this does not impact the measurement accuracy significantly because δ_{max} is still small. The parasitic torques exerted at the cradle bearings A and the load cell attachment B are estimated using the measured breakaway torque. Only the component of the torque along the cradle axis is considered and all other components assumed equal to zero.

Figure 24 is a contour plot of torque as a function of moment arm length (R) and load cell reading for a cell with a maximum rating of 80 oz (5 lb). The dashed lines are contours of uncertainty in the measurement based on a root-mean-square

average of the combined effects of the uncertainties in the parameters presented in table 3. The primary source of uncertainty in the torque measurement arises from the 0.21% of full scale (FS) uncertainty in the load cell reading. Accordingly, the figure indicates that the best accuracy is obtained by choosing a moment arm length that maximizes the force exerted on the load cell. The difficulty, of course, is that often the torque is not known until after the experiment is performed. Replacing the 80 oz cell with a more sensitive unit would permit the measurement of smaller torques to better than 0.5%. How small depends on the capacity of the sensor and the magnitude of the breakaway torque. Smaller cells are easier to damage and somewhat larger cells have been used to increase robustness.

3.7.2 Fuel Flow Rate Measurement.

Fuel flow rate is measured in one of two ways depending on the engine being tested. In the case of the AP yellow jacket engine, the fuel flow rate is measured using an FMTD4 nutating microflow meter manufactured by DEA Engineering. The meter is a positive displacement type that produces a series of 5 V pulses each of which corresponds to the passage of 1/50 of a cm^3 of fluid. The fuel flow rate is determined by measuring the frequency of the flowmeter signal using a digital oscilloscope. The oscilloscope is programmed to make about 15 frequency measurements of the flowmeter signal and is synchronized with the measurement of the other channels connected to the data acquisition system. However for smaller engines, the pressure drop in this flowmeter was found to be too large causing intermittent disruptions in the fuel flow. This made it necessary to find an alternative method for measuring fuel flow to the smaller engines.

For the smaller engines considered in the study, the fuel flow rate is determined by making a series of measurements of the mass of the fuel in the fuel tank at regular intervals over a specified period of time - usually 30 seconds. A least squares fit is then performed on the readings to get the time rate of change of the weight of the fuel in the tank. This gives the fuel mass flow rate.

3.7.3 Speed Measurement.

Engine speed is measured using an 'off the shelf' system manufactured by ElectroSensors. It consists of a magnetic 'pulser' disc containing sixteen alternating poles that is attached to the hystereris brake shaft, a proximity switch that detects the passage of these poles, and a model SA420 signal conditioner that outputs an analog voltage proportional to frequency. The accuracy of this system is +/- 0.1% of the reading.

3.7.4 Air flow measurement.

Air flow rate is measured using a TSI model 4021 mass flowmeter that has an operating range of 0-300 standard L/min and a linear 0-4 V DC output signal. The sensing element is a hot wire which is a type of a thermal anemometer. The pressure drop in the air flow setup as mentioned earlier is small (on the order of 0.01%). A thermal anemometer measures gas flow by sensing changes in heat transfer rate from a small, electrically heated element (in this case a wire) exposed to the flow. The element is held at a constant temperature using an electronic control circuit. The cooling effect of the gas flowing past the sensor is compensated for by increasing the electrical power to the sensor. The magnitude of power required to keep the sensor at

a constant temperature is proportional to the mass flow rate of the gas and inversely related to the temperature of the gas. This follows from King's law which is frequently used in mass flow measurements using thermal anemometry[52, 53, 54]. A temperature sensor is mounted upstream of the flow sensor to measure the gas temperature. The mass flow rate measurement can be calculated from these two signals.

3.7.5 Fuel pressure.

The fuel pressure in the tank is monitored using an Omega PX139 series differential pressure transducer with a range of ± 103.4 kPa (15 psi). The fuel pressure sensor is attached using tubing to a port on the fuel tank.

3.7.6 Temperature measurements.

Cylinder head temperature is measured using a stainless steel sheathed K type thermocouple held in contact with one of the cylinder head bolts. A similar thermocouple inserted into the muffler exit measures exhaust gas temperature.

3.8 Computed quantities.

3.8.1 Power Output.

At a stable operating point, the power produced by the engine is equal to the power absorbed by the brake or the engine torque (Γ) times its rotational speed (ω) in radians/sec.

$$P = \Gamma \omega \tag{12}$$

In terms of engine revolutions/minute:

$$P = \frac{\Gamma * 2\pi N}{60} \quad \text{since} \quad N = \omega \frac{60}{2\pi}$$

3.8.2 Thermodynamic Efficiency.

The overall thermodynamic efficiency of the engine is the ratio of the power output of the engine to the input power in the form of chemical potential energy in the fuel. This is also referred to as fuel conversion efficiency. It is given by[55]:

$$\eta_o = \frac{P}{\dot{m}_f Q_r} \tag{13}$$

where $\dot{m}_f$ is the mass flow rate of fuel in kg/s and Q_r is the lower heating value of the fuel in J/kg.

3.8.3 Brake Specific Fuel Consumption.

Brake specific fuel consumption is often preferred over thermal efficiency as a method of comparing engine performance. It is defined as the ratio of fuel consumption to the power output of the engine. It is measured in k/KW-hr or lb/hp-hr. It is expressed as[56]:

$$BSFC = \frac{\dot{m}_f}{P} \tag{14}$$

A typical value for a conventional-scale piston engine like the Lycoming IO 370 is 0.45 lb/hp-hr or 0.3 kg/kW-hr[62].

3.8.4 Delivery Ratio.

This is an important parameter that describes the volumetric efficiency of the engine. It compares the actual air mass flow rate through the engine to a reference

value which is the mass that would be ingested in an ideal intake process. It is the engine displacement times the ambient air density[57]:

$$\Lambda = \frac{\text{mass of delivered air per cycle}}{V * \rho_o} = \frac{\dot{m}_a}{V * \rho_o * \frac{N}{60} * r} \tag{15}$$

r = 1 for 2-stroke engine

r = ½ for 4-stroke engine

3.8.5 Fuel/Air Ratio.

Fuel/Air ratio is computed on a mass basis. It is calculated from the measurements of the air and fuel mass flow rates into the engine using the following relation:

$$F/A = \frac{\dot{m}_{fuel}}{\dot{m}_{air}} \tag{16}$$

3.8.6 Equivalence Ratio.

This parameter is of key importance in estimating the efficiency of the combustion process and directly affects the overall engine performance. It is the ratio of the fuel to air in the engine charge divided by the fuel to air ratio associated with stoichiometric combustion, ie. complete oxidation of all carbon and hydrogen in the fuel. The equivalence ratio is expressed as[58]:

$$\phi = \frac{(F/A)_{actual}}{(F/A)_{stoichiometric}} \tag{17}$$

For lean mixtures: $\phi < 1$

For an ideal mixture: $\phi = 1$

For rich mixtures: $\phi > 1$

A lean mixture refers to a fuel/air mixture having more air than is required for the complete combustion of the ingested quantity of fuel. A rich mixture refers to a fuel/air mixture that has lesser amount of air than that is required for complete combustion of the ingested quantity of fuel.

3.9 Data Acquisition.

A Lab View data acquisition system is used to condition and log signals from all of the sensors. Analog signals are amplified and low-pass filtered using a National Instruments SCXI 1327 instrumentation amplifier. Thermocouple signals are amplified using a National Instruments SCXI 1112 thermocouple amplifier. Analog to digital conversions are performed using an eight channel, 16 bit card resident in a PC. Pulses from the flow meter are counted using a TDS 3034B digital oscilloscope and converted into flow rate using the sensor's calibration factor. Acquisition of data from the oscilloscope is also controlled through the Lab View software. Figure 25 shows a picture of the LABVIEW user interface used to set user inputs and record engine data.

Data from the dynamometer is recorded in one of two modes. In the default strip chart mode, the channels are scanned once per second and the data are written to a file which provides a record of everything that happened in the course of an experiment. These data are also written to virtual indicators and strip charts displayed on a software panel to provide real-time graphical indications of the state of the experiment.

The difficulty with this mode of operation is that the timing of the scans is accomplished through software. Since other processes compete for CPU cycles, the true time elapsed between channel scans will not be constant. While this variability is small, it is not acceptable in the fuel flow rate measurement using the scale because the true time elapsed between measurements is not constant. In addition, the 1 Hz sampling rate of the strip chart mode is insufficient to acquire the large number of samples needed to do proper averaging and uncertainty analysis.

As a result, a button on the panel is provided which causes the software to enter a 'burst' mode of operation in which a fixed number of samples is acquired using a hardware trigger to ensure consistent timing intervals. Each burst consists of 1000 samples per channel acquired at 1 kHz. When the 'burst' is complete, the software returns to 'strip chart' mode. The 'burst' mode is used to acquire a large number of samples at a single operating point that can subsequently be averaged to reduce uncertainties associated with random error processes. When the burst is complete, the software returns to 'strip chart' mode.

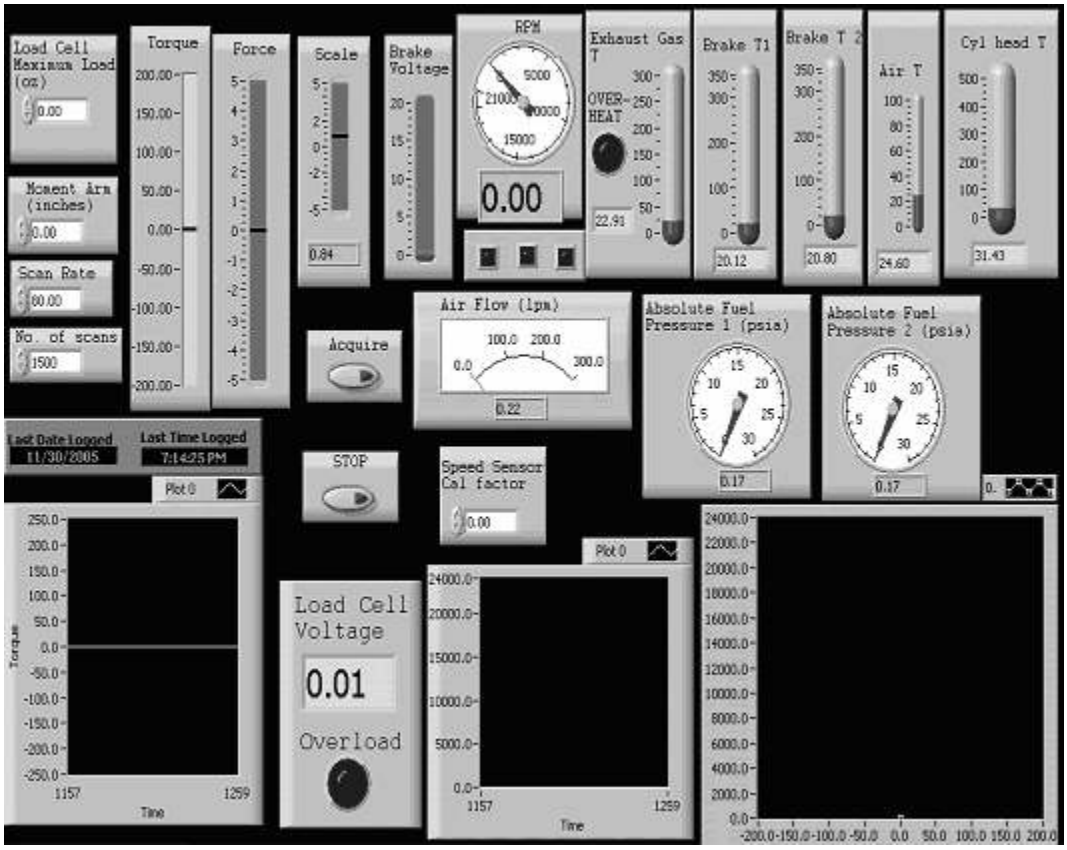

Figure 25 Picture of the LABVIEW GUI used to monitor engine data during the run.

3.10 Vibration Control.

The intermittent pressure pulses in the combustion chamber lead to strong 1/rev (1/2rev for 4 stroke engines) disturbances that can excite resonances in the cradle-load cell system. These disturbances decrease the signal-to-noise ratio of the measurement and if left unchecked can damage or destroy the load cell. As a result, the dynamic behavior of the cradle/load-cell system is another important consideration. The equation of motion of the cradle about its axis of rotation is:

$$\left(\Gamma_e + A\cos(\omega t)\right) - \beta\dot{\theta} - k_{lc}R^2\left(\theta - \theta_0\right) = I\,\ddot{\theta} \qquad (18)$$

where Γ_e is the steady component of the torque and $A\cos(\omega t)$ is the time-varying component of the engine torque. k_{lc} is the stiffness of the load cell, R is the position of

the load cell attachment relative to the cradle's axis of rotation, and β represents the damping by the cradle bearings. Changing variables by introducing $\phi = \theta - \theta_0 - \theta_e$ and noting that $\Gamma_e - k_{lc} R^2 \theta_e = 0$ in the steady state transforms equation 18 to the well known harmonic oscillator

$$I\ \ddot{\phi} + \beta\dot{\phi} + k_{lc} R^2 \phi = A\cos(\omega t) \tag{19}$$

with natural frequency given by

$$\omega_n = \sqrt{\frac{k_{lc} R^2}{I}} \tag{20}$$

The engine speed (in rpm) associated with the natural frequency of the cradle-load cell system is:

$$N_{nat} = \frac{60}{2\pi}\omega_n \tag{21}$$

Ideally, the engine-cradle system would be designed so that N_{nat} is significantly greater than N_{max}, the engine's maximum operating speed, so that resonances of the cradle/load cell system could not be excited. In practice, however, keeping ω_n high is difficult because the physical size of the engine places a lower bound on the total moment of inertia I. Meanwhile the load cell is relatively compliant and any structure associated with the cradle increases I and lowers ω_n further.

The approach taken here is to increase the moment of inertia of the system so that the operating speed of the engine corresponds to a high order mode of the cradle-load cell system that will be more highly damped. This is accomplished by adding pairs of weights that are directly opposite the cradle's axis of rotation (so that I is

increased but the center of mass is not affected). The overall moment of inertia becomes

$$I = I_e + I_c + mr^2 \tag{22}$$

where mr^2 accounts for the additional weight added to the cradle. In the latter term, m is the mass of the extra weight added to increase the overall moment of inertia and r is the distance from the cradle's axis of rotation at which this weight acts. While this strategy is not ideal because the engine must traverse the fundamental frequency as it accelerates to operating speed, locking the cradle down and releasing it after the engine has reached operating speed has prevented resonance-induced damage to the sensor. Table III shows the values of the constant terms in equations 19, 21 and 22.

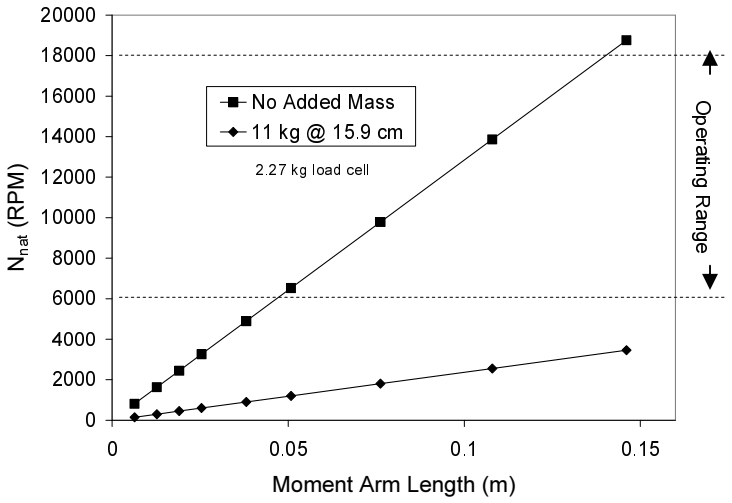

Figure 26 Engine RPM associated with the first resonant mode of the cradle-load cell system for various moment arm lengths. Increasing the cradle's moment of inertia pushes the fundamental frequency below the operating range of the engine.

Figure 26 is a plot of equation 20 as a function of moment arm length. It shows that N_{nat} can be pushed below the normal operating range of the engine by adding mass to the cradle and by decreasing the length of the moment arm. Both

strategies are pursued here: 5.4 kg has been added to the cradle at 6.25 inches from the cradle's axis of rotation, and a moment arm of 1.5 inches is used.

Chapter 4: Experimental procedure.

4.1 Engine break-in.

Prior to testing the engine on the dynamometer each new engine is broken in following the procedures recommended by its manufacturer. This involves running the engine on a test stand with the appropriate "break-in" propeller. The mixture is adjusted as per the manufacturer's instructions. The glow plug charger is connected to the glow plug and the engine is started using an electric starter motor. The mixture needle valve is set to a rich position initially and after a few minutes of running rich, it is set to a leaner setting after which the needle is adjusted to a rich setting for a few minutes. This is repeated for about 30 minutes. The main purpose of breaking in an engine is to smooth out the working surfaces of the engine parts and to align them to ensure efficient and safe operation of the engine[59]. An engine that has been broken-in properly also gives a quick, smooth acceleration and idles stably.

4.2 Calibration.

The torque measuring system is calibrated before and after each experiment. This is accomplished by running the data acquisition program and attaching a series of known weights to the moment arm at known locations. A data 'burst' is acquired for each new application of weights so that random fluctuations can be averaged out. Typical results are presented in figure 27. They show that the calibration of the torque measurement system is linear but that it does shift slightly after the engine has been run. The chief cause of this drift is the repositioning of connecting tubes and

other non-rigidly held apparatus during the experiment due to the vibrations caused by the engine run. This drift has been included in the uncertainty analysis.

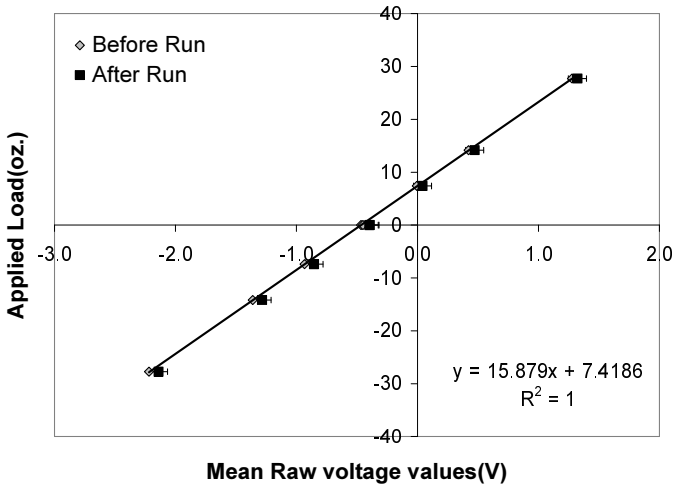

Figure 27 Typical load cell calibration data before and after a run.

4.3 Engine Startup.

The operation and control of all the engines tested on the dynamometer follow very similar patterns. The engine is started on the dynamometer by adjusting the mixture to the manufacturer recommended setting for starting, attaching the glow plug charger and turning the engine using an electric starter motor - this time via the dynamometer gearing. Because the propeller is no longer mounted on the engine, cooling air is provided by a blower. Engine load is applied using a hysteresis brake and the details the dynamometer operation will be discussed later on. The speed and power output of the engine are controlled by using a needle valve that changes the fuel-air mixture ratio and a throttle valve that controls the quantity of air entering the engine. The cradle is locked using a retaining screw prior to starting the engine. This allows ensures the safety of the load cell while the engine passes through the low

speed regime where resonant frequencies of the system could be excited. The retaining screw is removed and the cradle unlocked at a sufficiently high speed (>7000 rpm) where the performance measurements are made.

4.4 Operation.

4.4.1 Uncontrolled operation.

Once the engine is started, the cradle is unlocked and the engine is leaned according to the manufacturers' instructions. This is performed at wide open throttle (WOT) and involves closing the needle valve that meters the fuel until the engine speed peaks, and then retarding it by about ¼ turn. Failing to re-open the valve can cause the engine to operate too lean and overheat. In one case, operating too lean actually burned a hole through a piston.

Once the engine is leaned, the throttle is opened to the desired setting and both the throttle and the mixture setting are held constant. Initially the current supplied to the hysteresis brake is zero which simulates the no-load condition. The brake current is then varied to apply different loads to the engine. Once the engine speed has stabilized after a change in the brake current, a burst of data from all of the sensors is acquired. Power, efficiency, delivery ratio and equivalence ratio are computed using equations 12, 13, 15 and 16 respectively. The data required to generate power curves are acquired by measuring torque and engine speed at different loads. Unlike conventional dynamometers, no speed control (achieved by adjusting either the throttle position or the load) is applied. As mentioned previously, the engine has stable and unstable operating regimes and all the measurements made here are done

in the stable operating regime. As the applied load increases, the engine reaches a point where its operating point switches over into the unstable regime and at this point the engine begins to stall. Engine performance in this regime has to be characterized using a load controller in a feedback loop. This is proposed in the future work section of the thesis.

4.4.2 Controlled operation.

In this mode of operation, the throttle setting remains constant but the load and mixture settings are varied manually in order to maintain a constant engine speed. The speed to be maintained is initially set using the mixture control with no load applied. Any increase in the load causes a decrease in the engine speed. This is countered by leaning the mixture and thus getting the speed back up to the set value. This is repeated manually for operating points in the stable regime. These measurements are repeated for different engine speeds in order to determine the optimum fuel flow rate at different engine speeds.

4.5 Engine shutdown.

The cradle is re-locked to the cradle support before the fuel is exhausted or the engine is shut down. This prevents possible damage to the load cell as the engine decelerates and the speed passes through the fundamental resonant frequency of the cradle-load cell system. After the engine stops, the cradle is unlocked and a second calibration of the torque measuring system is performed.

4.6 Uncertainty Analysis.

A thorough analysis of the measurement uncertainty requires a rigorous understanding of the nature of the errors and a clearly defined method of estimating the uncertainty level. A discussion of the types of errors and the procedures for estimating uncertainly levels is presented in this section. It follows the guidelines proposed in ASME standard PTC19.1[60]. We begin with some definitions.

Measurement Error:

The difference between the true value and the measured value. Measurement error consists of two components: Systematic Error and Random Error. Both of these need to be minimized for accurate measurement.

Random Error:

The part of the measurement error which changes every time the true value is measured. The two main sources of random errors in the test setup are vibration in the cradle and noise in the signals from each sensor. Random error can be reduced by averaging.

Systematic Error:

The portion of the total measurement error that remains constant in repeated measurements. The elemental systematic error sources in the experimental setup include errors due to the linearity and repeatability limits of the various instruments used in the test as well as the offset in the signal output by the data acquisition system.

Uncertainty:

The sum of the uncertainties due to systematic and random errors.

Uncertainty due to Random errors:

Random errors are estimated from statistical variations in the measurements. The standard deviation, σ is a measure of the scatter about the true mean, μ caused by random error. The standard deviation of a data sample, S_x is given by:

$$S_{\bar{x}} = \frac{1}{\sqrt{M}} \sqrt{\sum_{k=1}^{M} \frac{(x_k - \bar{x})^2}{M-1}} \tag{23}$$

Where M is the number of measurements made and $\overline{X}$ is the mean of the individual measurements X_k given by:

$$\overline{X} = \frac{1}{M} \Sigma_{k=1}^{M} X_k \tag{24}$$

Uncertainty due to Systematic Error:

The total systematic uncertainty in a measurement is the root-mean-square sum of the contributions $b_1, b_2, \ldots b_m$ from various aspects of the measurement:

$$B = \sqrt{(b_1)^2 + (b_2)^2 + \ldots\ldots + (b_M)^2} \tag{25}$$

Total Uncertainty:

The total uncertainty is the sum of the uncertainties due to systematic and random errors. The true value of the measurement is defined to lie in an interval with a certain level of confidence. This interval is given by:

$$\overline{X} \pm U \tag{26}$$

where $\overline{X}$ is the measurement mean and U is the deviation from the mean..

For 95% confidence, U is given by

$$U = 2\sqrt{\left(\frac{B}{2}\right)^2 + \left(S_{\bar{x}}\right)^2} \tag{27}$$

where B represents the total systematic uncertainty in the measurement and S_x represents the contribution to the uncertainty from random processes. The latter can be minimized by averaging a large number of measurements. In this work, M=1000. The determination of overall uncertainty requires separate procedures to be followed for analyzing the uncertainty in the measurements and uncertainty in the quantities computed from the measurements.

Uncertainty of a computed result:

Most of the engine performance metrics (eg. Torque, power, efficiency and even load cell force and speed) are not measured directly. Instead they are computed from other fundamental quantities like voltage. Therefore, uncertainties in both the measured voltage and the proportionality constants used to infer force, speed etc. influence the overall uncertainty in the fundamental measurements. These fundamental measurements are subsequently used to compute quantities are to uncertainties in the fundamental measurements depends on how they are used in the calculation. The generalized method for propagating uncertainties through calculations is as follows:

For a generalized result $R = f(\overline{p}_1, \overline{p}_2, ..., \overline{p}_j)$, the total uncertainty in R is given by:

$$U_r = \sqrt{(\Theta_1 * u_1)^2 + (\Theta_2 * u_2)^2 + ... + (\Theta_j * u_j)^2} \tag{28}$$

$$\Theta_j = \frac{\partial R}{\partial \overline{p}_i} \tag{29}$$

where u_j is the uncertainty in the quantity $\overline{p}_j$ and Θ_j is the sensitivity coefficient of f with respect to $\overline{p}_j$.

Equations 23-27 are used to determine the uncertainties in all of the voltage measurements. Equations 28 and 29 are used to determine the uncertainties in all computed such as force, torque, speed, fuel flow rate, fuel pressure, temperature, engine power and efficiency. Sample results from the uncertainty analysis are presented in Table IV. They show that uncertainty in the force measurement is the most important contributor to uncertainty in the power measurement while uncertainty in the fuel flow rate is the most important contributor to uncertainty in the efficiency measurement.

	Value	Uncertainty	Unit	% Uncertainty
F_{lc}	1.598	0.135	N	8.45
ω	10009.12	27.86	rpm	0.278
$\dot{m}_f$	0.1269	0.00095	gm/s	0.75
P	63.58	5.4	W	8.5
η_o	2.29	0.204	%	8.9

Table IV Results of uncertainty analysis for a typical engine performance point.

4.7 Atmospheric corrections.

Since engine performance varies with the number of oxygen molecules per unit volume in the atmosphere which varies depending upon the local pressure,

temperature, and humidity, engine performance is usually corrected to standard atmospheric conditions so that measurements made on different days may be compared. The methods for accomplishing this are well known[61] but we will summarize them here:

A correction factor α_c times the measured power P gives the power P_r corrected to standard reference conditions:

$$P_r = \alpha_c P \tag{30}$$

The correction factor for a naturally aspirated compression ignition engine depends on the atmospheric factor f_a and the engine factor f_m:

$$\alpha_c = (f_a)^{f_m} \tag{31}$$

The atmospheric factor accounts for the effects of atmospheric pressure p, temperature T and humidity ϕ and is computed as follows:

$$f_a = \left(\frac{p_r - \phi_r p_{sr}}{p - \phi p_s} \right) \left(\frac{T}{T_r} \right)^{0.7} \tag{32}$$

The subscripted terms correspond to the reference conditions and the non-subscripted terms correspond to test conditions.

The engine factor for a 2-stroke engine is[61]:

$$f_m = 0.036 q_c - 1.14 \tag{33}$$

$$q_c = q / r_r \tag{34}$$

where q is the fuel mass per cycle per liter of air (set by the fuel/air ratio) and r_r equals 1 for the loop-scavenged engines considered here.

Chapter 5: Results.

5.1 Time history.

Figures 29 and 30 show the time history of some of the sensor readings accumulated in the strip chart file over the course of a typical experiment without any kind of control. Figure 29 shows engine torque and speed. Figure 30 shows plots of exhaust gas, cylinder head, hysteresis brake and ambient air temperatures as well as the command voltage applied to the hysteresis brake power supply. Since increasing the command voltage to the brake increases the load on the engine, the latter curve provides a visual indication of the load cycle applied to the engine. The engine is started under no-load conditions so the initial engine speed is high – about 11500 RPM. Engine speed then decreases as the load is applied.

The relatively large fluctuations in the torque shown in figure 29 are a result of vibrations in the system and demonstrate the importance of averaging large numbers of samples to reduce the random component of the error. The flat spots on the brake command voltage trace show where the engine was allowed to come to equilibrium with the load and where bursts of data were acquired for the purpose of averaging. These averaged values are used to compute the power and efficiency curves of the engine.

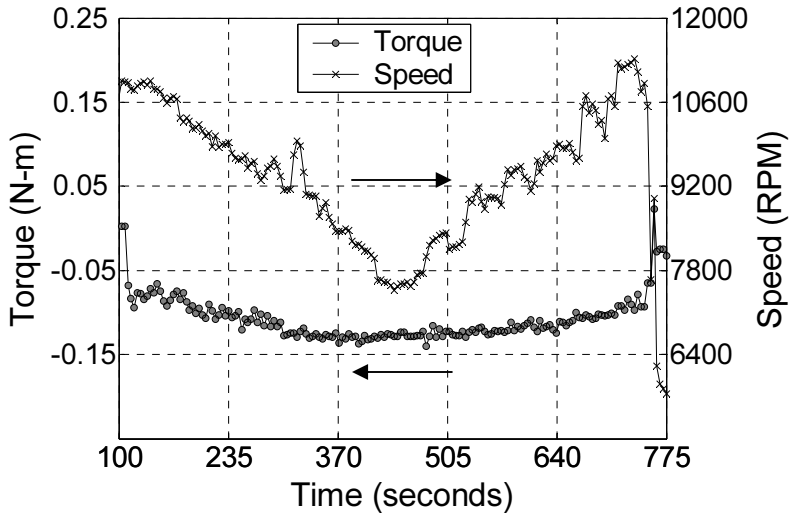

Figure 29 Time history of engine torque and speed. The throttle is fully open and the mixture is leaned per factory instructions.

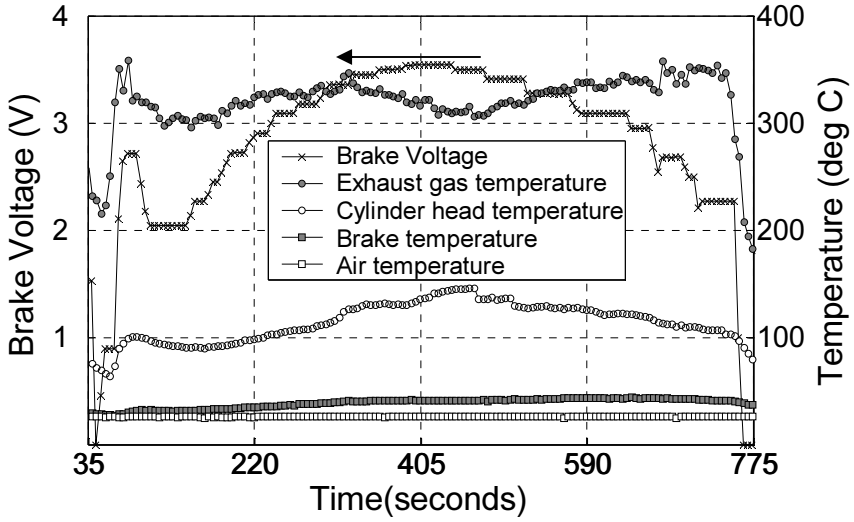

Figure 30 Time history of brake temperature, cylinder head temperature, exhaust gas temperature, room temperature and brake voltage from a test of the AP Yellowjacket engine.

The temperature of the hysteresis brake rotor rises over the course of the experiment as the power produced by the engine is converted to heat in the brake which is dissipated via transfer to the environment. As the engine speed decreases, the fuel/air ratio decreases and there is a higher heat release per power stroke. This raises the cylinder head temperature. The temperature measured by the exhaust gas

thermocouple, however, is strongly influenced by heat transfer processes in the muffler. At lower speeds, the residence time in the muffler is higher and there is more time for the exhaust gases to lose heat. As a result, lower engine speeds actually result in lower temperatures of the gas exiting the muffler even though the temperature of the gas entering the muffler (from the cylinder) is higher.

5.2 Instrument repeatability.

The repeatability of the dynamometer is verified by making three sets of measurements of the Yellowjacket engine performance curves at the same operational settings while correcting for the variations in atmospheric conditions prevalent during each test. Figure 28 shows engine torque, corrected power, fuel/air ratio (mass basis) and efficiency at wide open throttle (WOT) as a function of engine speed. Data are presented from three separate experiments in which the mixture setting was adjusted per the engine manufacturer's instructions. The data show that torque decreases monotonically with increasing engine speed while corrected power output peaks near the middle of the operating range around 10,000 RPM. The fuel flow rate increases with engine operating speed because bleed gases from the exhaust manifold are used to pressurize the fuel tank. The increase in fuel flow rate is faster than the increase in air flow rate and the net result is the linear increase in fuel/air ratio with engine speed shown in the figure. While this could be advantageous (and possibly necessary) from the point of view of engine cooling, it significantly reduces the engine's overall efficiency. The overall efficiency peaks at approximately 8% at 7500 RPM and decreases linearly with engine speed. The overall efficiency at peak power is

approximately 6%. These numbers are much lower than the approximately 30% overall efficiency achieved by general aviation engines when properly leaned[62].

The data are repeatable within their respective uncertainty intervals with the torque measurement showing both the largest uncertainty and the largest variation between experiments. The majority of the variation between experiments is caused by the drift in torque sensor calibration occurring over the course of an experiment and small variations in needle-valve adjustment between runs. An additional contributor is variations in atmospheric conditions which are not accounted for in the torque data presented in figure 28. However, variations in atmospheric conditions are accounted for in the power measurements and as a result, the variability in power is somewhat less. Overall, however the dynamometer system appears to be repeatable enough to characterize changes in engine performance with operating speed and engine size.

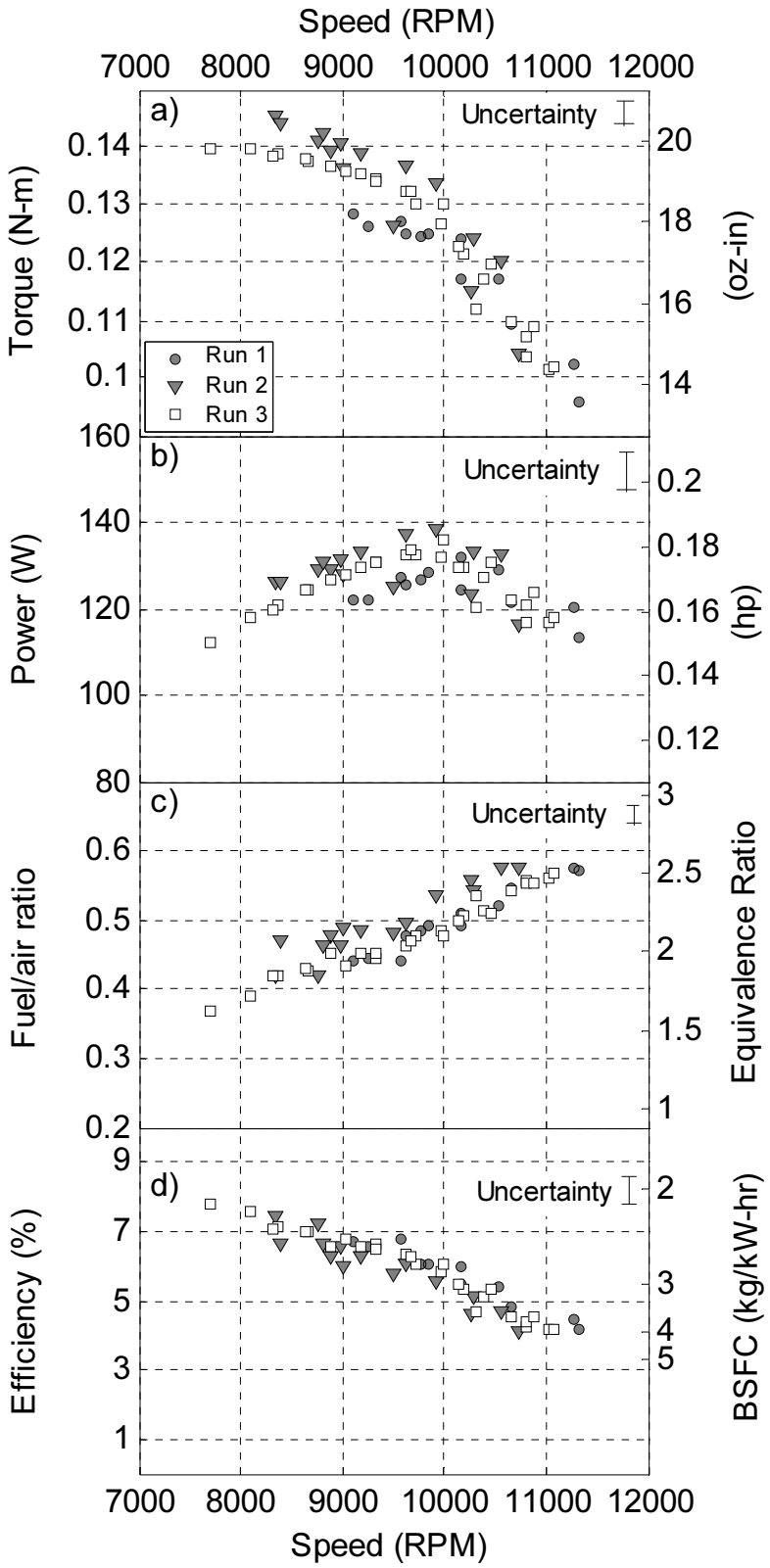

Figure 28 Engine performance map for AP engines Yellowjacket at constant mixture setting and WOT showing repeatability between 3 runs conducted on different days.

5.3 Effect of mixture setting.

Figure 31 shows engine performance as a function of engine speed at WOT for two different mixture settings. The purpose of this was to investigate the engine performance in a wider range than the manufacturer suggested operating conditions. The 'Factory' mixture setting corresponds to a run where the mixture is set per the engine manufacturer's instructions (~1.5 turns) while the 'Rich' setting corresponds to a run where the mixture valve is opened more widely (2 turns) so that the fuel/air ratio is higher than normal. Less torque and power are produced under these conditions because the combustion temperature is lower and therefore the pressure in the cylinder is lower. The reduction in combustion temperature is reflected in lower exhaust gas temperatures (EGT) as illustrated in figure 32. The data also show, as expected, that increasing the mixture setting (ie. richening the mixture) increases the fuel/air ratio and decreases the engine efficiency.

Finally, it should be pointed out that the measurements presented in figure 28 are significantly different from those associated with the 'Factory' setting in figure 31 in spite of the fact that in both cases, the mixture was adjusted according to factory instructions. The reason is that following the factory instructions – which tell the operator to adjust the mixture for maximum RPM (as determined by the engine sound) and then open the mixture valve a specified amount (in this case ¼ turn) – does not lead to very repeatable needle valve settings. The results presented in figure 28 were obtained by taking great care to ensure that the mixture valve opening was the same for all three experiments.

Table V compares engine performance parameters measured at 9600 RPM for the two different mixture settings. Leaning the mixture increases torque, power, efficiency, and exhaust gas temperature.

Parameter	Lean	Rich	Unit
Mixture setting	1.5	2	Turns
Torque	0.1473	0.0902	N-m
Power	0.109	0.0667	HP
Efficiency	4.19	2.54	%
Exhaust Gas T	216.22	197.15	Deg C
Fuel/Air Ratio	0.48	0.57	

Table V Change in AP Yellowjacket engine performance with mixture setting at 9600 RPM.

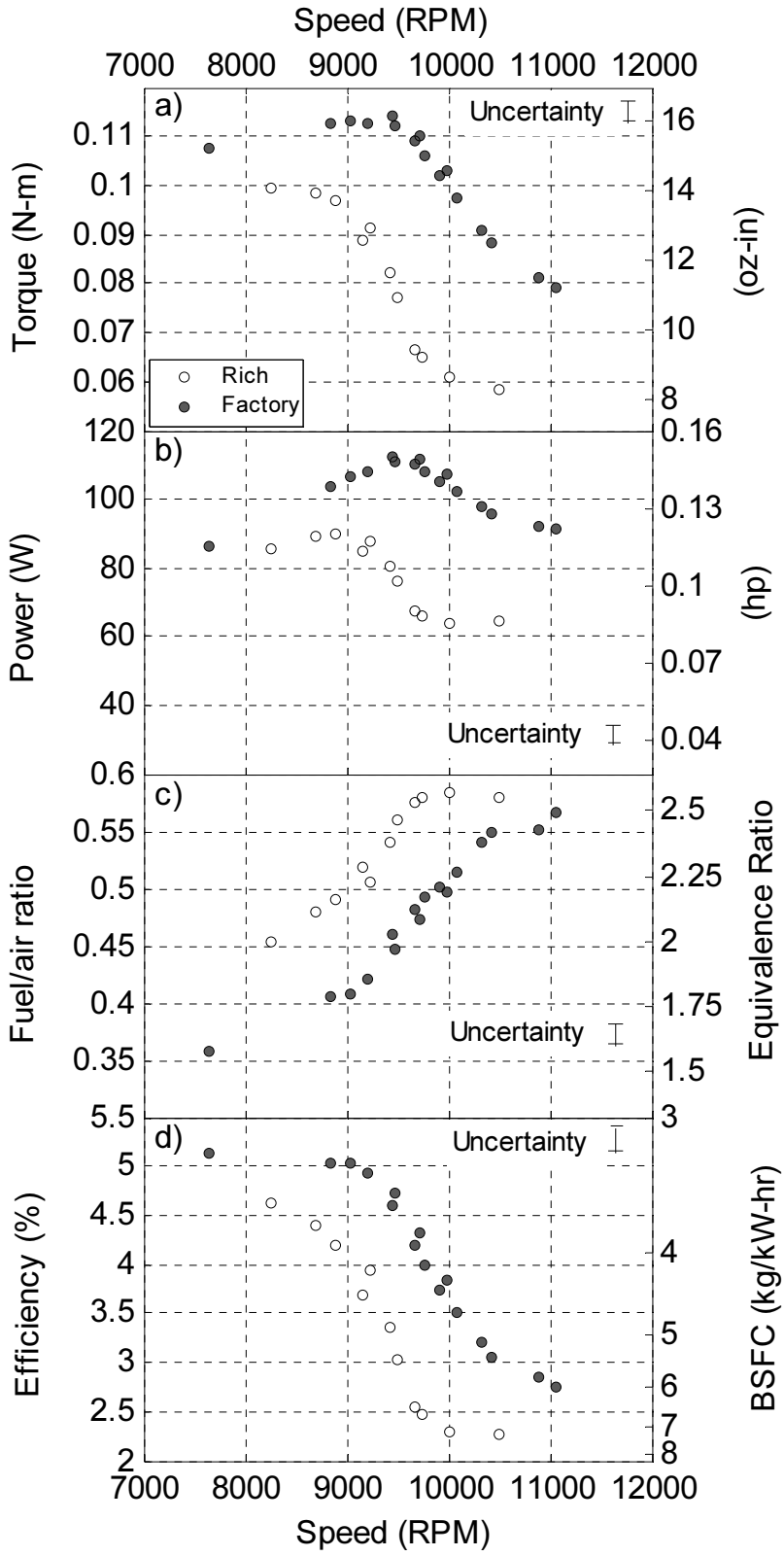

Figure 31 Engine performance map for AP engines Yellowjacket at different mixture settings and WOT.

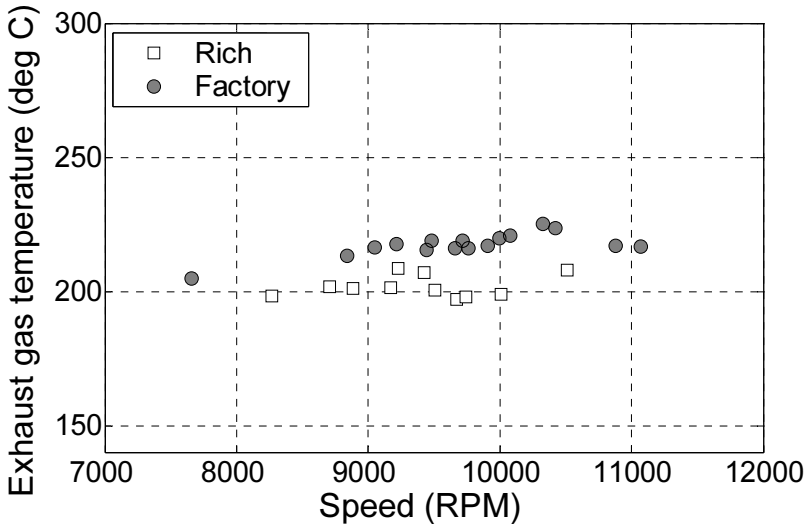

Figure 32 Exhaust gas temperatures for two different mixture settings of AP engines Yellowjacket.

Figures 28 and 31 show that power and torque decrease with increasing speed over most of the engine's operating range. This trend is opposite to what one usually sees in conventional-scale engines where the power and torque increase approximately linearly with RPM before tailing off at the engine's maximum rated speed. One reason for this behavior is that the overall volumetric efficiency of the engine decreases with increasing engine speed thereby reducing the amount of oxygen available for reaction in the combustion chamber. This is illustrated in figure 33 which shows that the "delivery ratio". Figure 33 suggests that less energy is released per stroke at higher speeds because less air (oxygen) is available to react with the fuel. The result is reduced torque and eventually reduced power. As expected, the delivery ratio is independent of the mixture setting.

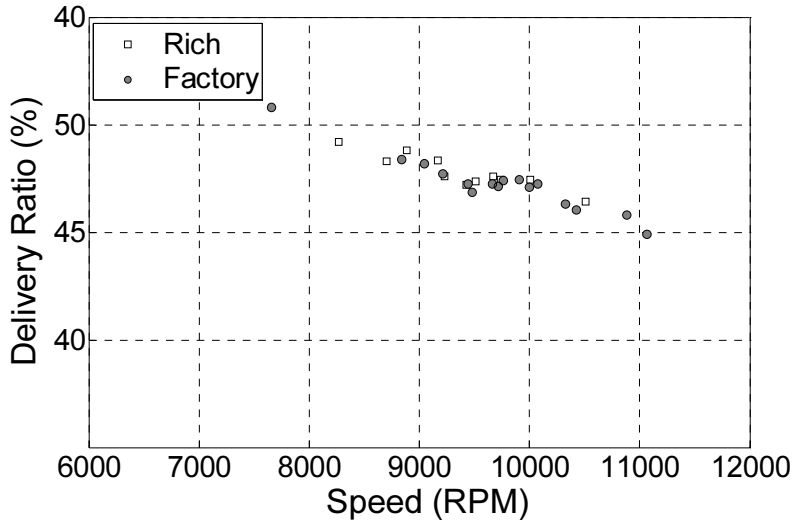

Figure 33 Delivery ratio as a function of engine speed at WOT for two different mixture settings.

If no oil burns in the cylinder, the cylinder head temperature should peak at a fuel/air ratio of 0.23 (mass basis) that corresponds to stoichiometric combustion of the methanol and nitromethane in the fuel with air. Figure 34 shows cylinder head temperatures (CHT) increasing monotonically with decreasing fuel/air ratio. However the minimum fuel/air ratio in the test is still higher than the stoichiometric value where the temperature would be expected to peak. Thus, the mixture appears to be rich everywhere. This value of fuel/air mixture is computed assuming no combustion of oil. Assuming the oil burns completely reduces the stoichiometric value for the fuel/air mixture to about 0.14. Therefore, if the cylinder head temperature peaks at a fuel/air ratio lower than 0.23, it suggests that a significant fraction of the oil actually burns in the cylinder and that the equivalence ratio is greater than 1 (ie. rich) over a large portion of the engine operating range. The decrease in torque with engine speed illustrated in figure 31 is related to the decrease of the overall Damkohler number (or the ratio of the time available for combustion to the time required to complete the chemical reaction) with increasing engine speed. Lower Damkohler numbers mean

less of the fuel reacts before it leaves the combustion chamber, chamber temperatures are lower, chamber pressures are lower, and consequently torque is lower.

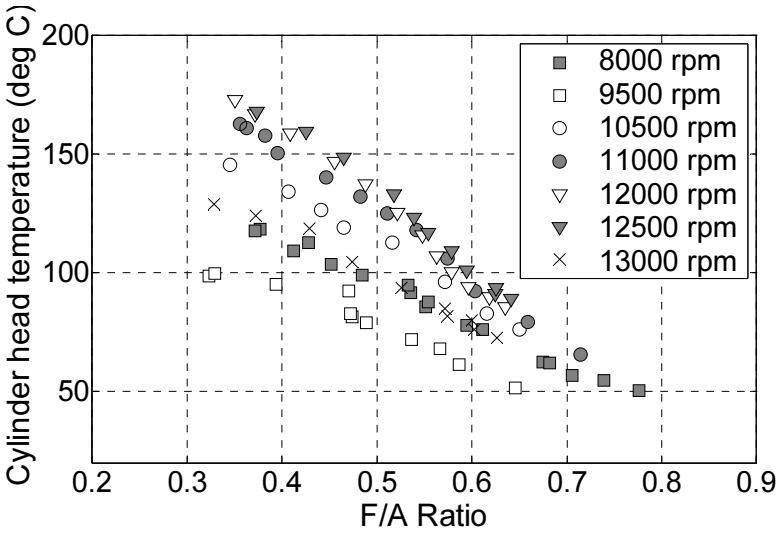

Figure 34 Cylinder head temperature as a function of fuel/air ratio at WOT.

The results presented so far illustrate that the engine's performance is heavily influenced by the fuel/air ratio which changes significantly over the operating range of the engine. Therefore, a final set of measurements was made to identify the optimum mixture settings associated with various operating speeds. This was accomplished by varying the mixture setting using the needle valve while adjusting the load to maintain constant engine speed.

The fuel/air mixture ratio shows a linear variation with changes in the needle valve setting for many different operating speeds as shown in figure 35. The figure also shows the average value of the fuel pressure measured in the tank for each operating speed. Fuel pressure increases with increasing RPM and peaks at around 12,500 RPM.

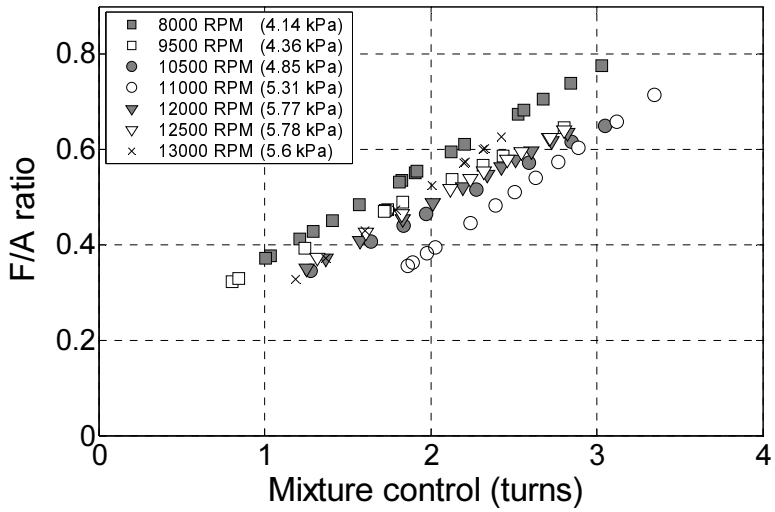

Figure 35 F/A ratio as a function of mixture setting for different engine speeds and the corresponding fuel pressure.

The engine performance measurements corresponding to controlled operation at different speeds is presented in figure 36. This kind of presentation could enable the operator of the MAV to determine the optimum engine operating conditions for a particular flight condition. The engine condition corresponding to best power would be used for climb whereas the one corresponding to best fuel consumption would be used to achieve best cruise performance. The results show that the peak power output of the engine is 159 W at 12,000 RPM. This is slightly greater than the value measured with the fixed needle valve setting. Since the power output doesn't change much between 10,500 RPM and 12,000 RPM, the data indicate that it may be advantageous to operate at 10,500 RPM in applications where engine life is important. The peak power density of the engine is 1060 W/kg which is comparable to that of a 'typical' general aviation engine like the Lycoming IO-370-2LA (134.4 kW, 133.8 kg).

Figure 36 shows that fuel/air ratio decreases with engine speed. Fuel/air ratio would be expected to be increase at higher speeds due to increasing fuel pressure that drives more fuel into the engine. However, in addition to fuel pressure, fuel consumption is governed by the mixture control valve. The drop in fuel flow rate due to the closure of the valve is higher than the increase caused by higher fuel pressure and the net effect is to reduce fuel/air ratio at higher speeds when operated at a constant throttle position.

BSFC approaches the same limiting value of 2 kg/kW-Hr (corresponding to an efficiency of 8.3%) at all operating speeds - a 37% improvement over the value obtained without mixture control. Since aircraft range and endurance are directly proportional to engine efficiency, these data suggest that controlling the mixture offers the potential to significantly improve UAV range and/or endurance. An optimum fuel/air ratio would be one that gives highest possible efficiency with least potential damage to the engine due to overheating. In addition, the fact that the minimum BSFC can be obtained at all operating speeds is advantageous because it means that tradeoffs between efficiency and power output are not required. However this overall level of efficiency (8%) is still much lower than that achieved by conventional-size aircraft engines. For example, the Lycoming IO-370-2LA has a specific fuel consumption of 0.27 kg/kw-Hr[62] which corresponds to an overall efficiency of approximately 30%. As a result, an MAV powered by the small engine tested here will be unable to achieve levels of range and/or endurance comparable to those achieved by larger vehicles with more efficient powerplants.

Finally, a careful examination of the data presented in figure 37 shows that the power output of the engine does, in fact, increase with engine speed (like conventional-size engines) at constant mixture ratio. Therefore, the unusual shapes of the power curves presented in figures 28 and 31 (i.e. the decrease in power with engine speed) are a direct result of the variation in mixture ratio with engine speed. This can be seen more clearly in figure 37 which shows peak power and fuel/air ratio as a function of engine speed. The data show that peak power occurs when the fuel/air ratio is held constant at a value of approximately 0.4. Peak power decreases rapidly beyond speeds of 12,000 RPM because of decreases in volumetric efficiency and Damkohler number.

5.4 Implication for UAV operation:

Nevertheless, this level of performance is still advantageous when compared to the performance of UAVs powered using batteries or fuel cells. The range of a small, fixed-wing UAV can be expressed in terms of the efficiency of the power plant η_{th}, along with the efficiency of the propulsion system (propeller) η_p, the heating value of the fuel Q_R, the lift/drag ratio of the vehicle, and the fuel mass fraction at takeoff χ_f using the Brequet range equation[12]:

$$R = \eta_p \eta_{th} \frac{Q_R}{g} \left(\frac{L}{D} \right) \ln\left(1 + \chi_f\right) \tag{35}$$

Table VI shows the range of various vehicles computed using equation 35 for a 'typical' small UAV with L/D = 8, η_p=0.7 and χ_f=0.45. The data show that improvements in range and/or endurance of approximately 35% can be achieved by implementing some sort of mixture control.

Power System	η_{th}	Q_R	Range	Endurance (at 30 m/s)
Li-Polymer Battery with electric motor[63]	95	333	218	2
DARPA direct methanol fuel cell (1000 W-hr/kg) with electric motor[64]	35	1000	267	2.47
150 g model engine (standard)	6	6061	278	2.57
150 g model engine with mixture control	8.2	6061	380	3.5
	%	W-Hr/kg	Km	Hr

Table VI Effect of power system choice on small UAV range and endurance.

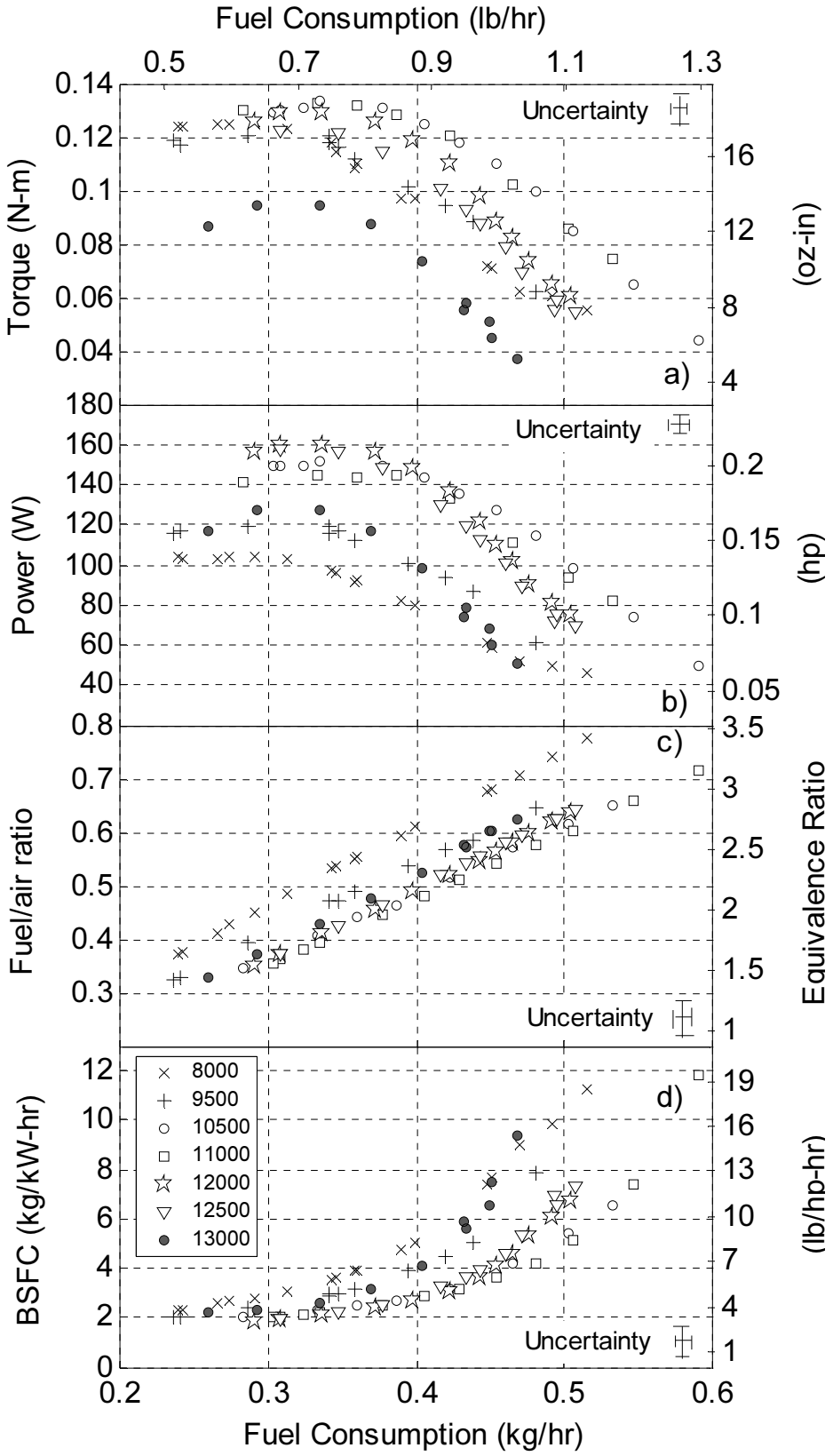

Figure 36 Summary of engine operating map at different engine speeds and WOT.

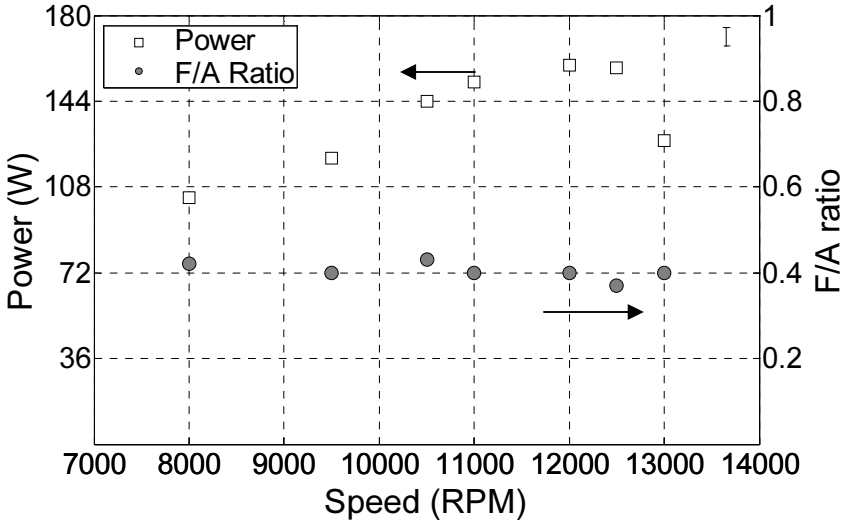

Figure 37 Peak power output and corresponding fuel/air ratio as a function of engine speed at WOT.

5.5 Performance Scaling.

An additional objective of this work is to understand the nature of the scaling of engine performance and losses with size. However, special care needs to be taken when selecting engine operating conditions at which different engines are compared. The reason is that the results presented earlier show that engine power output and efficiency vary widely over the operating range of the engine. Therefore, comparing a randomly selected performance point of one engine to a randomly selected point of another would make it very diffcult to draw meaningful conclusions about engine performance scaling. A comparison of engine power output to isolate the effects of size can be reasonable only if the performance metrics across different engines are compared at constant throttle position, engine speed and at a similar fuel/air mixture ratio. When these factors are kept constant, the change in performance across different engines is solely the result of changing engine size (or combustion volume). Since loss mechanisms (heat and frictional losses) are a function of size as well, such a study would highlight the effects of engine scaling on them. Tests producing results

similar to those presented in figure 36 were done on the Norvel BigMig and the AP Hornet engine. The smaller fuel flow in these engines required the use of the scale for fuel flow measurement. However, the measurements obtained were not of good quality due to effects of vibration and extraneous noise on the voltage signal from the scale. Torque and power were however measured at a range of constant engine speeds and at WOT. In the absence of fuel flow (and hence fuel/air mixture) data, another approach would be to use exhaust gas temperature data for comparing performance measurements. Power output from each engine at constant speed and WOT can be obtained at the peak exhaust gas temperature across the run. This point would have the stoichiometric fuel/air mixture which is constant for all engines as they burn the same fuel. This approach also fails in this case as no clear peak exhaust gas temperature is established for any run. A controlled dynamometer would allow this kind of measurement to be made as data points to the left of the torque peak (where the stoichiometric point seems to lie) could be acquired.

As a first approximation, we use the peak temperature point as obtained from the uncontrolled run to find a qualitative estimate for the scaling of engine power. Figure 38 shows power output plotted as a function of cylinder surface/volume ratio for all three engines operating at a speed of 11000 rpm. The data is taken for the maximum exhaust gas temperature recorded for that speed. A power law is fit to the data.

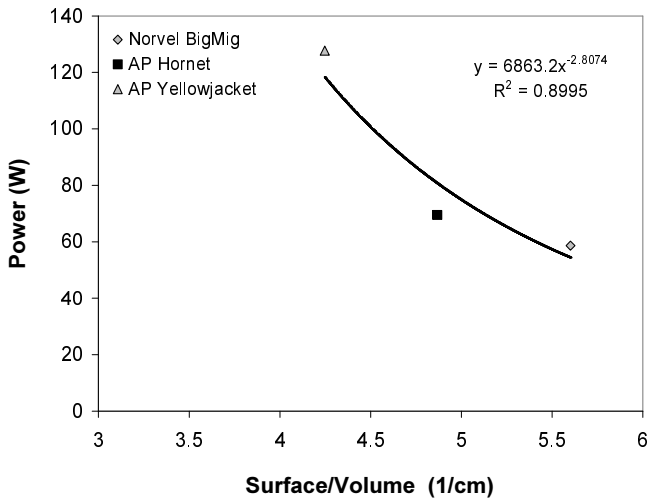

Figure 38 Engine power as a function of surface to volume ratio for constant engine speed (11000 rpm), throttle position (WOT) and fuel-air mixture (stoichiometric).

Figure 39 presents the similar preliminary measurements presented in figure 38 in the larger context of about 40 IC engines ranging in size from 13g to 1000g. The diamonds correspond to these engines' peak power as reported by their manufacturers[11] while the squares correspond to the measurements made in this study. The first thing to notice is that power output tends to decrease with engine size and that that a power law seems to be a reasonable model for how power output scales with engine size. However, the power outputs measured here seem to be lower than the estimates for the other 40 engines and the power output tends to increase more slowly with size than one would expect based on the manufacturers' data. This could mean that engines follow a different scaling law at small scales. One reason for this could be the different fuels that are used in testing the engines. Even with model airplane fuel, fuel mixtures might contain differing amounts of nitromethane and oil. Another reason is that manufacturers may use different standards when reporting power. Also the manufacturer data used here is for peak engine power. At small

scales, the difference in power output with engine rpm is relatively larger as compared to conventional engines and hence peak power does not form a good enough basis for comparison. Whatever the origin of the discrepancy, however, the figure highlights the importance of developing scaling laws based on well-understood performance measurements.

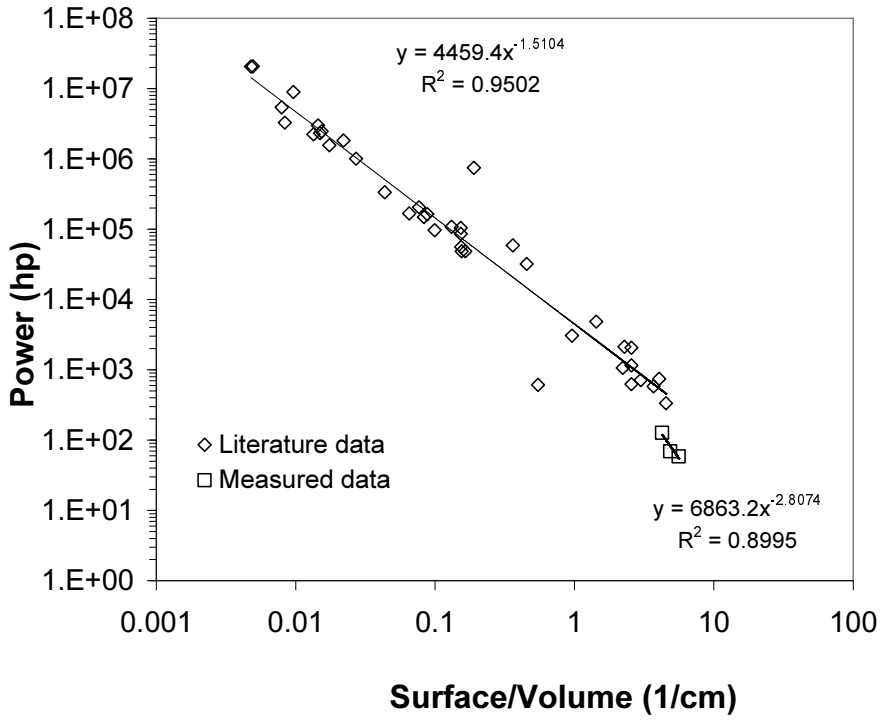

Figure 39 Scaling of small IC engine power output.

Chapter 6: Conclusions and Future Work.

6.1 Conclusions.

A dynamometer system suitable for measuring the performance of small internal combustion engines has been constructed. It has been shown to be capable of measuring power output within +/- 9% and BSFC (or overall efficiency) within +/- 9%. This level of fidelity is sufficient to resolve the differences in performance between engines of different sizes to enable the development of scaling laws for small engine performance. The peak power output of the AP Engines Yellowjacket is 159W (0.2 HP) at 12,000 RPM. This is 15% lower than the manufacturer's estimate of 0.25 HP but corresponds to a power density of 1060 W/kg which is comparable to that of a conventional-size piston aero engine. However, the overall efficiency of the stock engine is approximately 6% which is almost four times lower than the 30% achieved by conventional-scale piston aero engines. This dramatic reduction in efficiency at small-scales illustrates the difficulty of developing small UAVs with levels of range and/or endurance comparable to larger-scale vehicles and demonstrates the importance of understanding the factors that govern how engine performance scales with size. However, the data also indicate that improving the fuel delivery system by implementing some sort of mixture control can increase overall efficiency to 8%. This, in turn, could increase range and/or endurance of a small UAV by approximately 40% compared to a comparable battery-powered vehicle.

Detailed measurements of the performance of two other small 2-stroke IC aero engines were also made on a small dynamometer system. The measurements show that a power law relationship seems to govern the scaling of engine power

output with size. While this is consistent with earlier findings, it is important to note that the power levels measured in this work are consistently lower than those reported by manufacturers of similar size engines. Also the nature of the power law seems to be different at smaller scales with the power output decreasing at a faster rate with decrease in engine size. However, further investigation and measurement data from more engines are required to establish this fact.

6.2 Future Work.

Future work on the dynamometer will concentrate on extending the investigation of the scaling of engine size with power and efficiency. Engines belonging to a range of sizes will be tested to determine if the scaling relationship obtained from literature for bigger engines hold in the small engine regime. Measurements will be made at fixed air-fuel ratios across engines to get more insight into the scaling. Compression ratio will also be investigated in this respect as a controlling parameter. Measurements will also be extended to two-stroke engines running on diesel fuel with variable compression ratio as well as to glow engines converted to diesel engines using special conversion heads. Both these types of engines offer potential for use in future UAV systems. A control system will also be implemented to acquire engine data in the low rpm regime. Attempts will be made to build an engine control device integrated with the engine to form a complete package for a viable power system.

Appendix A

Calculation of stoichiometric fuel/air ratio for a sample fuel composition considering no burning of oil:

Consider a sample of the fuel with the following volumetric composition:

CH_3OH – 70 %; CH_3NO_2 – 10%; Oil – 20 %

Hence,

$$\chi_{CH_3OH} = 0.7;\ \chi_{CH_3NO_2} = 0.1;\ \chi_{Oil} = 0.2$$

The volume of the fuel sample is 5 cc.

The volume of each component is given by:

$$V_i = \chi_i * V_{mixture}$$

The mass of each component is hence given by:

$$m_i = V_i * \rho_i$$

The number of moles of each component is given by,

$$N_i = \frac{m_i}{MW_i}$$

The above set of calculation for this sample of fuel yields the following results:

$$N_{CH_3OH} = 0.088;\ N_{CH_3NO_2} = 0.009;\ N_{Oil} = 0.003$$

We consider that the oil remains inactive during the combustion process. The balanced chemical reaction for the complete combustion of the fuel with air is then given by:

$$(aCH_3OH + bCH_3NO_2 + cOil) + x(0.21O_2 + 0.79N_2) \Rightarrow (a+b)CO_2 + \frac{(4*a+3*b)}{2}H_2O + cOil + (x*0.79)N_2$$

The set of constituents in the first parenthesis is the fuel and the one in the second is air.

Here, a = 0.088; b = 0.009; c = 0.003.

The number of moles of air required for complete combustion (x) is then given by:

$$x = \frac{\left(2*(a+b) + \frac{(4*a+3*b)}{2} - a*1 - b*2\right)}{0.42}$$

This calculation for the given sample of fuel yields:

x = 0.668

The mass of air required for complete combustion is given by:

$$m_{air} = N_{air} * MW_{air}$$

The mass of fuel in the given sample is given by:

$$m_{fuel} = N_{CH_3OH} * MW_{CH_3OH} + N_{CH_3NO_2} * MW_{CH_3NO_2} + N_{Oil} * MW_{Oil}$$

The stoichiometric fuel/air ratio by mass is then given by:

$$F / A_{stoich} = \frac{m_{fuel}}{m_{air}}$$

For the given sample of fuel, the stoichiometric fuel/air ratio by mass works out to:

$$F / A_{stoich} = 0.227$$

For the given sample of fuel, the heating value (in kJ assuming no oil to be burnt) is given by:

$$Q_R = m_{CH_3OH} * Q_{CH_3OH} + m_{CH_3NO_2} * Q_{CH_3NO_2}$$

Heating value of the fuel (per gram of fuel) is given by:

$$\bar{Q}_R = \frac{Q_R}{m_{fuel}}$$

Calculation of stoichiometric fuel/air ratio for a sample fuel composition considering 100% of oil to be burnt:

Consider a sample of the fuel with the following volumetric composition:

CH_3OH – 70 %; CH_3NO_2 – 10%; Oil – 20 %

Hence,

$$\chi_{CH_3OH} = 0.7;\ \chi_{CH_3NO_2} = 0.1;\ \chi_{Oil} = 0.2$$

The volume of the fuel sample is 5 cc.

The volume of each component is given by:

$$V_i = \chi_i * V_{mixture}$$

The mass of each component is hence given by:

$$m_i = V_i * \rho_i$$

The number of moles of each component is given by,

$$N_i = \frac{m_i}{MW_i}$$

The above set of calculation for this sample of fuel yields the following results:

$$N_{CH_3OH} = 0.088;\ N_{CH_3NO_2} = 0.009;\ N_{Oil} = 0.003$$

We consider that the oil remains inactive during the combustion process. The balanced chemical reaction for the complete combustion of the fuel with air is then given by:

$$(a*(CH_3OH) + b*(CH_3NO_2) + c*(C_{18}H_{34}O_3)) + x(0.21*O_2 + 0.79*N_2)$$

$$\Rightarrow (a+b+18*c)CO_2 + \frac{(4*a+3*b+34*c)}{2} H_2O + (x*0.79)N_2$$

The set of constituents in the first parenthesis is the fuel and the one in the second is air.

Here, a = 0.088; b = 0.009; c = 0.003.

The number of moles of air required for complete combustion (x) is then given by:

$$x = \frac{\left(2*(a+b+18*c)+\frac{(4*a+3*b+34*c)}{2}-a*1-b*2-c*3\right)}{0.42}$$

This calculation for the given sample of fuel yields:

$$x = 1.056$$

The mass of air required for complete combustion is given by:

$$m_{air} = N_{air} * MW_{air}$$

The mass of fuel in the given sample is given by:

$$m_{fuel} = N_{CH_3OH} * MW_{CH_3OH} + N_{CH_3NO_2} * MW_{CH_3NO_2} + N_{Oil} * MW_{Oil}$$

The stoichiometric fuel/air ratio by mass is then given by:

$$F / A_{stoich} = \frac{m_{fuel}}{m_{air}}$$

For the given sample of fuel, the stoichiometric fuel/air ratio by mass works out to:

$$F / A_{stoich} = 0.1438$$

For the given sample of fuel, the heating value (kJ) is given by:

$$Q_R = m_{CH_3OH} * Q_{CH_3OH} + m_{CH_3NO_2} * Q_{CH_3NO_2} + m_{C_{18}H_{34}O_3} * Q_{C_{18}H_{34}O_3}$$

Heating value of the fuel (per gram of fuel) is given by:

$$\bar{Q}_R = \frac{Q_R}{m_{fuel}}$$

Bibliography

[1] Prospective Unmanned Aerial Vehicle Operations in the Future National Airspace System Matthew DeGarmo* and Gregory M. Nelson† AIAA 4th Aviation Technology, Integration and Operations (ATIO) Forum 20 - 22 September 2004, Chicago, Illinois

[2] A Design Approach For Low Cost, "Expendable" Uav Systems, Cameron Munro Petter Krus, AIAA's 1st Technical Conference and Workshop on Unmanned Aerospace Vehicles, S 20-23 May 2002, Portsmouth, Virginia

[3] http://www.acrtucson.com/UAV/silverfox/index.htm last downloaded 6/2/2005.

[4] http://www.northropgrumman.com/unmanned/index.html last downloaded 12/22/2005.

[5] Particle Swarm Optimization for ResourceAllocation in UAV Cooperative Control, J. Cruz, G. Chen, D. Li and X. Wang, Ohio State University, Columbus, OH AIAA-2004-5250 AIAA Guidance, Navigation, and Control Conference and Exhibit, Providence, Rhode Island, Aug. 16-19, 2004.

[6] Development of a Heavy Fuel Engine for an Unmanned Air Vehicle, J. Lawton, AIAAISAEIASMEIASEE 26th Joint Propulsion Conference July 16-18, 1990 *1* Orlando, FL

[7] Development Of Micro Air Reconnaissance Vehicle As A Test Bed For Advanced Sensors And Electronics, Qamar A. Shams, Thomas L. Vranas, Robert L. Fox, Theodore R. Kuhn, John Ingham, Michael J. Logan, Kevin N. Barnes, and Benjamin F. Guenther, AIAA's 1st Technical Conference and Workshop on Unmanned Aerospace Vehicles, S
20-23 May 2002, Portsmouth, Virginia

[8] Goldeneye: The Clandestine Uav Carl G. Schaefer, Jr., Lawrence J. Baskett, 2nd AIAA "Unmanned Unlimited" Systems, Technologies, and Operations — Aerospace 15 - 18 September 2003, San Diego, California.

[9] Improving Aerodynamic Efficiency of Small-Scale Airfoils By Surface Temperature and Heat Transfer Jongmin Kim, Zvi Rusak and Nikhil Koratkar, 21st Applied Aerodynamics Conference 23-26 June 2003, Orlando, Florida

[10] O'Meara, M. M., and Mueller, T. J., "Laminar Separation Bubble Characteristics on an Airfoil at Low Reynolds Numbers", *AI' Journal,* Vol. 25, NO. 8, pp. 1033-1041, August 1987.

[11] Hill, P. G., Peterson, C. R., 'Mechanics and Thermodynamics of Propulsion', Addison Wesley, 1965, p.145.

[12] Peterson, R. B., 'Size Limits for Regernerative Heat Engines', *Microscale Thermophysical Engineering*, 2, pp 121-131, 1998.

[13] Aichlmayr, H. T., D. B. Kittelson, and M. R. Zachariah, "Miniature Free-Piston Homogeneous Charge Compression Ignition Engine-Compressor Concept-Part I: Performance Estimation and Design Considerations Unique to Small Dimensions," Chemical Engineering Science Vol. 57 No 19, pp. 4161-4171, 2002.

[14] McMahon, T, and Bonner, J, On Size and Life, Scientific American Library 1983, p. 61-62.

[15] Judge, Arthur. W., "The testing of high speed internal combustion engines." Chapman and Hall ltd., 1955, p.160.

[16] "Understanding Diesel Combustion Through The Use Of High Speed Moving Pi-tures In Color", SAE paper 690002, SAE Trans. Vol. 78, 1969..

[17] " Relation between fuel injection and heat release in a direct-injection engine and the nature of the combustion processes", Auste, A.E.W. and Lyn, W., Proc.Institution -of Mech. Engineers, No.1, pp 47-62, 1960-61.

[18] "A gas sampling study on the formation processes of soot and NO in a DI diesel engine", Aoyagi, Y., Kamimoto, T., Matsui, Y., and Matsuoka, S., SAE paper 800254, SAE Trans., vol.89, 1980.

[19] David Shawcross, Colin Pumphrey & David Arnall, "A Five-million Kilometre, 100-Vehicle Fleet Trial, of an Air-Assist Direct Fuel Injected, Automotive 2-stroke Engine", SAE paper 2000-01-0898.

[20] "OS Engines, Max-46 AX, Owner's manual", pg.31, http://www.osengines.com/manuals/46ax-manual.pdf, last downloaded 03/07/2006.

[21] Cadou, C. P., Moulton, N., and Menon, S., "Performance Measurement and Scaling in Small Internal Combustion Engines", 41st AIAA Aerospace Sciences Meeting and Exhibit, AIAA 2003-0671, Reno NV, 6-9 January 2003.

[22] Chinn, P. G. F., "Import Review", Model Airplane News, Morris, pg. 28, 1957

[23] Gierke, David, " Nelson Quarter .40", *Model Airplane News*, Morris, Vol.126, Iss.12; pg.88.

[24] Gierke, David, "We test 10 .60 engines: Which is right for you?", *Model Airplane News*, Morris, Vol.131, Iss.5; pg.28.

[25] Chinn, Peter, “Engine Review O.S. Max 10 R/C”, Model Airplane News, Morris, pg. 24, August 1966.

[26] Chinn, Peter, “Engine Review Webra .61 R/C”, Model Airplane News, Morris, pg. 20, December 1976.

[27] Pond, Steve and Gierke, David, “O.S .18TZ – A weapon of mass combustion”, *Radio Control Nitro,* March 2005.

[28] Cadou, C. P., Sookdeo, T., Moulton, N., and Leach, T., “Performance Scaling and Measurement for Hydrocarbon-Fueled Engines with Mass Less than 1 Kg”, 1st AIAA Unmanned Aerospace Vehicles, Systems, Technologies, and Operations Conference, and Workshop, Portsmouth, VA May 20-22, 2002

[29] Gierke, David, “Part I Dynamometer and Engine Performance Analysis”, Flying Models, June, 1973, pg. 21-25.

[30] Gierke, David, “Part II Dynamometer and Engine Performance Analysis”, Flying Models, July, 1973, pg. 43-51.

[31] Gierke, David, “Part III Dynamometer and Engine Performance Analysis”, Flying Models, July, 1973, pg. 38-47.

[32] Gierke, David, C., “Two-stroke glow engines for r/c aircraft.”, Air Age Inc., 1994, p. 48.

[33] Papac, J., and Dunn-Rankin, D., ‘Combustion in a Centimeter-Scale Four-Stroke Engine’, paper 04S-11, Western States Section of the Combustion Institute, 2004.

[34] Papac, J. and Dunn-Rankin, D., ‘In Cylinder Pressure and Combustion measurements in a Miniature Reciprocating Engine’, 4th Joint Meeting of the U.S. Sections of the Combustion Institute, 2005.

[35] Rais-Rohani, M. and Hicks, G., ‘Multidisciplinary Design and Prototype Development of a Micro Air Vehicle’, AIAA Journal of Aircraft, 36, 1, pp. 227-234, 1999.

[36] Micro-Power Generation Using Combustion: Issues and Approaches A. Carlos Fernandez-Pello *Proc. Combust. Inst.,* 29 (2002) 883-899.

[37] Fuel efficiency and the physics of automobiles, MARC ROSS, *Contemporary Physics,* 1997, volume 38, number 6, pages 381 ± 394.

[38] Improving Aerodynamic Efficiency of Small-Scale Airfoils By Surface Temperature and Heat Transfer Jongmin Kim, Zvi Rusak and Nikhil Koratkar, 21st Applied Aerodynamics Conference 23-26 June 2003, Orlando, Florida

[39] "Development Of A Catalytic Silicon Micro-Combustor For Hydrocarbon-Fueled Power Mems", C. M. Spadaccini, X. Zhang, C. P. Cadou, N. Miki, and I. A. Waitz, *Sensors and Actuators A* 103 (2003) 219–224.

[40] Cadou, C. P., "Reactive Processes in Micro-scale Combustion Systems", Invited paper, Western States Section of the Combustion Institute, October 20-21, Los Angeles, CA 2003.

[41] H. T. Aichlmayr, D. B. Kittelson, D.B., M. R. Zachariah, Chem. Eng. Sci. 57 (19) (Oct 21 2002), 4161-4171.

[42] Annen, K. D., Stickler, D. B., and Woodroffe, J., ,Linearly-Oscillating Miniature Internal Combustion Engine (MICE) for Portable Electric Power', 41st Aerospace Sciences Meeting and Exhibit, Jan 6-9, 2003.

[43] Epstein, A. and Senturia, S. D. Macro Power from Micro Machinery. Science 1997, 276 1211.

[44] Fu, K., Knobloch, A., Martinez, F., Waktger, D., Fernandez-Pello, C., Pisano, A., Liepmann, D., Miyaska, K., Maruta, K., ,"Design and Experimental Results of Small-Scale Rotary Engines", Proceedings of the International Mechanical Engineering Conference and Exhibition, New York, 2001.

[45] "The two-stroke cycle engine", Heywood, J.B., Sher Eran, 1999, pg.9.

[46] "The two-stroke cycle engine", Heywood, J.B., Sher Eran, 1999, pg.4.

[47] ASME Standard, Standard test method for heat of combustion of liquid hydrocarbon fuels by bomb calorimeter, D240, 2002.

[48] Makovky, A., Lenji, L., "Nitromethane - physical properties, thermodynamics, kinetics of decomposition, and utilization as fuel", Chemical Reviews 58 (4): 627-644 1958.

[49] Judge, Arthur. W., "The testing of high speed internal combustion engines." Chapman and Hall ltd., 1955, p.160.

[50] Judge, Arthur. W., "The testing of high speed internal combustion engines." Chapman and Hall ltd., 1955, p.162.

[51] "Hysteresis brakes and clutches-User manual", Magtrol Inc., pg.3.

[52] King, L.V., On the convective heat transfer from small cylinders in a stream of fluid. Determination of convective constants of small platinium wires with application to hot-wire anemometry; Phil. Trans R. Soc.214A (1914), pp. 373-432.

[53] Andrews, G.E.; Bradley, D.; Hundy, G.F., Hot wire anemometer calibration for measurements of small gas velocities: Int. J. Heat Mass Transfer; Vol. 15, No. 10 (1972), pp. 1765- 1786.

[54] "Flow gas transducer in basis of a hot wire with a nickel-titanium alloy its flow calibration system, Carlos Andres Mugruza Vassallo.

[55] Heywood, J. B., "Internal Combustion Engine Fundamentals", McGraw-Hill Book Company, 1988, p. 52.

[56] Heywood, J. B., "Internal Combustion Engine Fundamentals", McGraw-Hill Book Company, 1988, p. 51.

[57] SAE Recommended Practice. "Engine Terminology and Nomenclature-General" in SAE Handbook, J604d.

[58] Heywood, J. B., "Internal Combustion Engine Fundamentals", McGraw-Hill Book Company, 1988, p. 71.

[59] Gierke, David, **"**Break-in: The secret to longevity and reliability", Model Airplane News, Nov 2001.

[60] ASME-PTC 19.1, ASME Test Standard, 1998.

[61] "Engine Power Test Code-Spark Ignition and Compression Ignition- Gross Power Rating", SAE J1995 Standard, June 1995.

[62] Cessna 172S Pilot's Operating Handbook, Cessna Aircraft Corp, 2003.

[63] A. Carlos Fernandez-Pello, "Micro-Power generation using combustion: Issues and Approaches", Proceedings Of The Combustion Institute, Vol.29, Part 1, 2002, pg 883-899.

[64] Yao SC, Fedder GK, Amon CH, Tang X, Hsieh CC, Alyousef YM, et al., "Thermo-fluids considerations in the development of a silicon-based micro-scale direct methanol fuel cell", ASME-ZSIS international thermal science seminar, Bled, Slovenia, 2004, p. 171–80.